IASI L2 Surface Temperature: PPF v5 Validation Results

Doc.No.	:	EUM/MET/TEN/10/0188
Issue	:	v1
Date	:	1 June 2010
WBS	:	

EUMETSAT
Eumetsat-Allee 1, D-64295 Darmstadt, Germany
Tel: +49 6151 807-7
Fax: +49 6151 807 555
http://www.eumetsat.int

Document Change Record

Issue / Revision	**Date**	**DCN. No**	**Changed Pages / Paragraphs**
v1	1 Jun 2010		First release.

Table of Contents

1 INTRODUCTION

1.1 Purpose and Scope

The sea and land surface temperature products (respectively SST and LST) are operationally produced by the IASI Level 2 (L2) Product Processing Facility (PPF) operated at EUMETSAT. They have been retrieved by a statistical method up to version v4.3.3 of the IASI L2 PPF, based on a regression in a principal components (PC) space of the IASI spectra, defined by the empirical orthogonal functions (EOF). This is commonly referred to as 'EOF regression' in this document. Some initial validation results have already been documented and published [RD 2] but these mainly addressed the central part of the IASI swath.

With the introduction of the PPF v5.0, the land surface temperature is now retrieved with an optimal estimation method (OEM), while the SST remains as the output of the EOF. This document records the validation results of these two parameters, which have been extended to larger viewing angles.

1.2 Document Structure

This document splits into five parts:

- Section 1: this introduction
- Section 2: SST validation results
- Section 3: LST validation results
- Section 4: discussion of results
- Section 5: summary and conclusions

1.3 Reference Documents

RD 1 Schlüssel, P., "EPS Ground Segment IASI Level 2 Product Generation Specification", EPS.SYS.SPE.990013

RD 2 August, Th. et al., "First validations of the operational IASI L2 surface temperature", EUMETSAT User Conference 2008

RD 3 "IASI L1 PCC Product Generation Specification", EUM/OPS-EPS/SPE/08/0199

RD 4 "EPS Product Validation Report: IASI L1 PCC PPF", EUM/OPS-EPS/REP/10/0148

RD 5 Corlett, G.K. et al. (2006), "The accuracy of SST retrievals from AATSR: An initial assessment through geophysical validation against in situ radiometers, buoys and other SST data sets", Advances in Space Research, Vol. 37, Issue 4, pp.764-769

RD 6 Noyes, E.J., P.J. Minnett, J.J. Remedies, G.K. Corlett, S.A. Good, D.T. Llewellyn-Jones (2006), "The accuracy of the AATSR sea surface temperatures in the Caribbean", Remote Sensing of Environment, Vol. 101, No.1, pp. 38-51

RD 7 Hultberg, T., "EPS Product Validation Report: IASI L1 PCC PPF", EUM/OPS-EPS/REP/10/0148

RD 8 Masuda, K., T. Takashima, Y. Takayama, 1988, "Emissivity of pure water and sea waters for the sea surface in the infrared window regions", Remote Sensing of Environment, 24, 313-329

RD 9 The GHRSST-PP International Project Office, "The GHRSST-PP Product User Guide"

RD 10 "(A)ATSR L2P Product Description", RAL-L2P-TN-001

RD 11 "IASI Level 1 Day-2 Product Validation Test Report", EUM/OPS-EPS/REP/10/0069

RD 12 "EPS Product Validation Report: IASI L1 PCC PPF", EUM/OPS-EPS/REP/10/0148

RD 13 "Single Sensor Error Statistic scheme for IASI Level 2 Sea Surface Temperature", EUM/MET/DOC/10/0123

RD 14 "Algorithm Theoretical Basis Document for Land Surface Temperature", LSA SAF, SAF/LAND/IM/ATBD_LST/1.0

RD 15 "SAF for Land Surface Analysis – Validation Report LST", LSA SAF, SAF/LAND/IM/VR_LST/I_08

RD 16 "Product User Manual – Land Surface Temperature", LSA SAF, SAF/LAND/IM/PUM_LST/2.4

RD 17 Zhou, D. et al., "Thermodynamic and cloud parameter retrieval using infrared spectral data", Geophysical Research Letters, Vol. 32, L15805, doi:10.1029/2005GL023211, 2005

RD 18 "IFS DOCUMENTATION – Cy33r1 ; Operational implementation 3 June 2008", ECMWF

RD 19 "Vertical temperature and humidity profiles within IASI L2 PPFv5: non-regression tests and validation results", EUM/MET/TEN/09/0448

1.4 Acronyms

AATSR	Advanced Along-Track Scanning Radiometer
AVHRR	Advanced Very High Resolution Radiometer
ECMWF	European Centre for Medium-Range Weather Forecasts
EOF	Empirical Orthogonal Function
FG	First Guess
IASI	Infrared Atmospheric Sounding Interferometer
IFOV	Instantaneous Field Of View
LSA	Land Surface Analysis
LST	Land Surface Temperature
L2	Level 2
MODIS	Moderate Resolution Imaging Spectroradiometer
NWP	Numerical Weather Prediction
OEM	Optimal Estimation Method
PC	Principal Components
PPF	Product Processing Facility
PSF	Point Spread Function
SAF	Satellite Application Facility
SEVIRI	Spinning Enhanced Visible and Infrared Imager
SST	Sea Surface Temperature

2 SEA SURFACE TEMPERATURE

The SST retrieval in the IASI L2 PPF v5 is performed with the same algorithm as in version 4 and is the result of a linear regression in a spectral EOF space [RD 1]. The only direct modification in PPF v5 in that area resides in the input radiances which are now noise-filtered before being processed by the retrieval function [RD 3 and RD 4]. Eventually, the cloud filtering which mostly relied on the so-called “Cloud Test A” [RD 1 §5.9] in PPF v4, a IASI window channel test, was strengthened with the additional use of the AVHRR cloud mask in PPF v5.

2.1 Comparison with AATSR

2.1.1 Data Description and Match-up Criteria

As with the IASI L2 PPF, the AATSR processor is designed to retrieve the surface skin temperature. The reference products are the L2 ATS_NR_2P made available on http://www.medspiration.org/ in the frame of the Global High-Resolution SST Pilot Project (GHRSST-PP). They have a horizontal resolution of 1 km and were validated against in-situ measurements (buoys and ships) and airborne radiometry. The retrieval algorithm includes atmospheric corrections covering multi-spectral and dual-angle view capability. The products are characterised by a bias of 0.05 K at night (0.1 K for daytime) and by a typical standard deviation of 0.25 K during night-time (0.35 K during day) [RD 5, RD 6].

The results of a case study running on six days, from 19 to 24 March 2010, are presented in this section. As for the collocation of AATSR pixels to IASI IFOVs, only the clear cases as identified in the IASI processing chain were retained where at least 200 good AATSR pixels (according to the L2 SST quality flags) could be found in a radius of 15 km around the IASI IFOV centre. Additionally, the match-ups were rejected if the standard deviation of AATSR SST exceeded 0.4 K in order to restrict to homogeneous scenes and limit the impact of the IASI PSF in the intercomparisons. It can also be noted that these last two criteria effectively act as an additional cloud test. A total of approximately 8×10^6 AATSR individual SST retrievals were eventually collocated to IASI and considered in this study.

2.1.2 Global Intercomparison Results

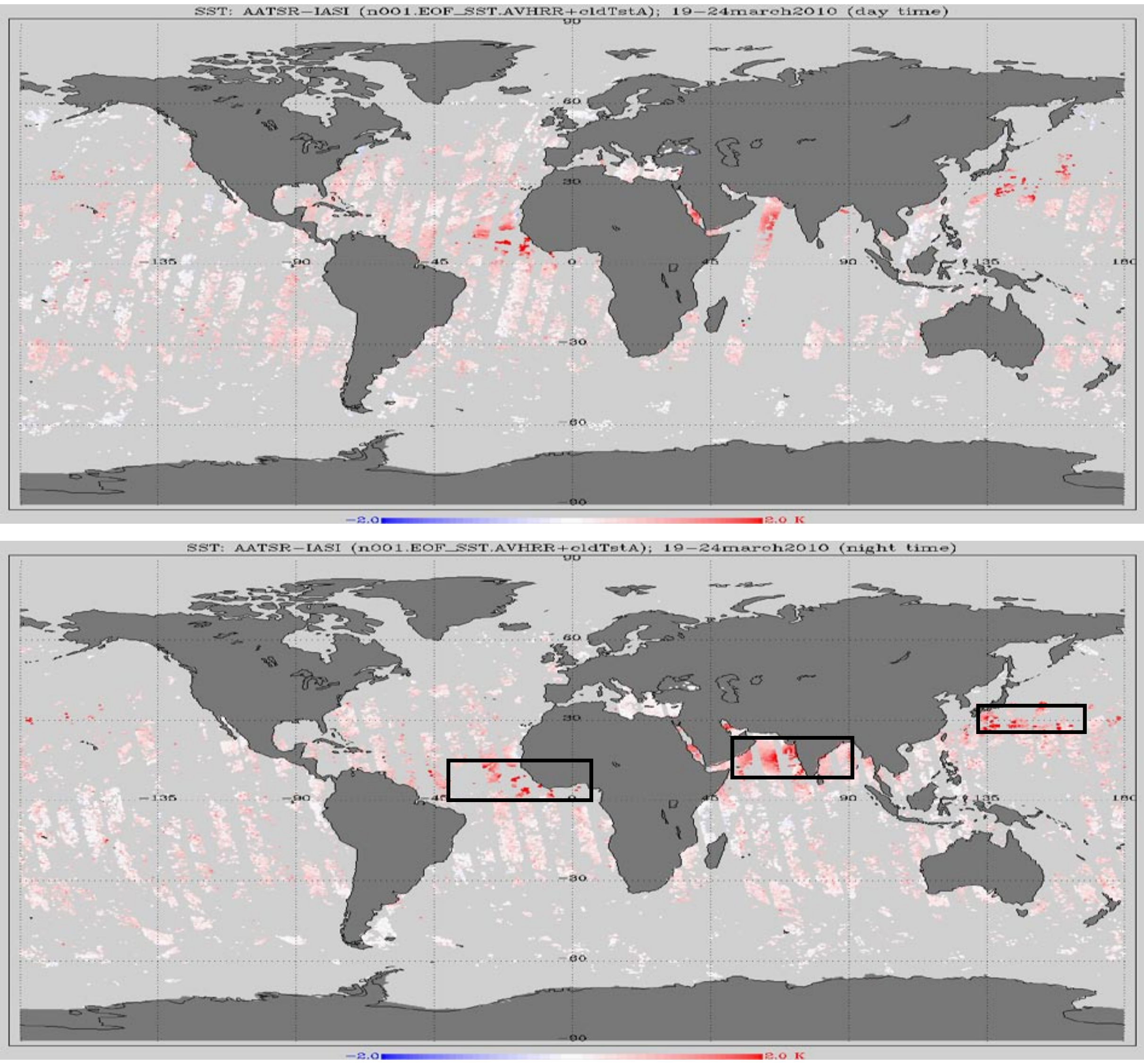

Figure 1: *(AATSR–IASI) SST mean departure for daytime (top) and night-time (bottom)*

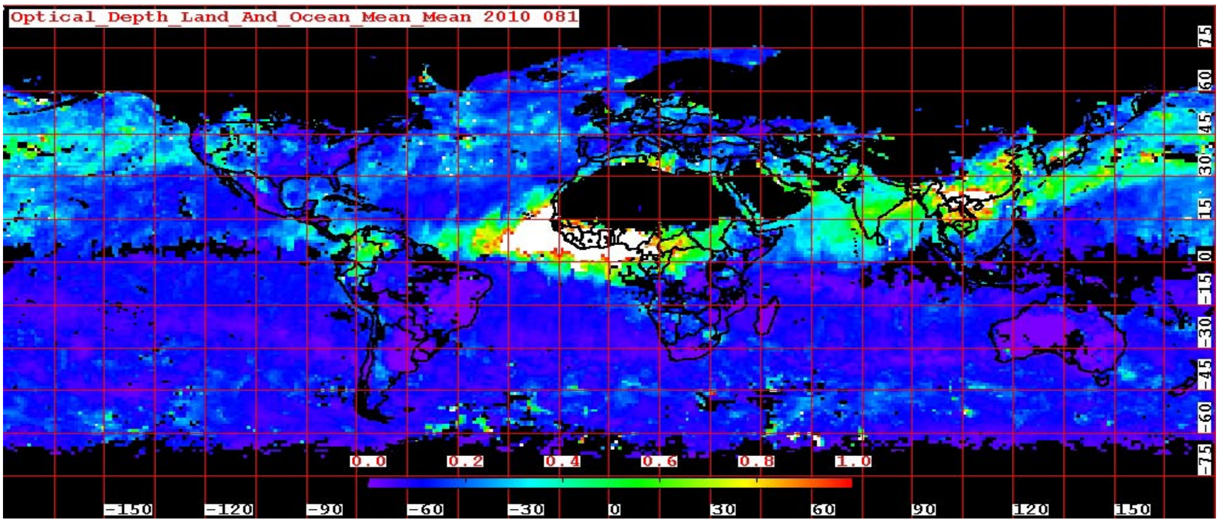

Figure 2: *MODIS aerosol optical depth, 22 March 2010*

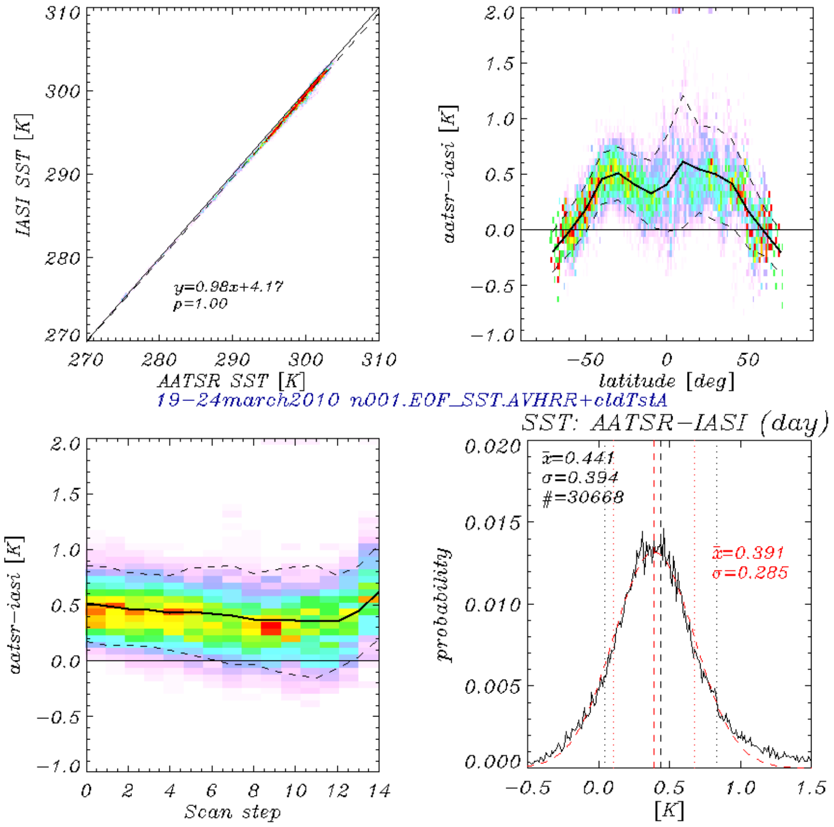

Figure 3: *(AATSR–IASI) SST statistics for daytime (above) and night-time (below). Clockwise, from upper left corner quadrant: AATSR vs. IASI correlation, AATSR–IASI variation with latitude, AATSR–IASI variation with scan angle and AATSR–IASI distribution.*

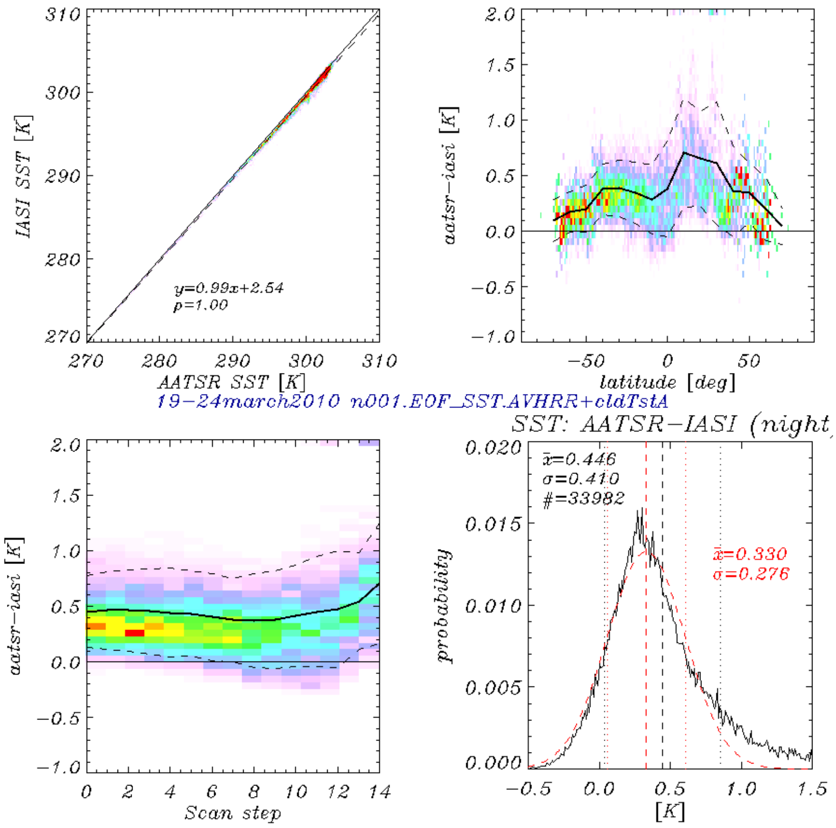

2.2 Comparison with ECMWF Analyses

2.2.1 Data Description and Match-up Criteria

The same IASI Level 2 products were compared to ECMWF six-hour analyses interpolated to the IFOV location and time. The ECMWF sea surface temperature (SST) is based on analyses received daily from NCEP, Washington, in a 0.5° x 0.5° grid and relies on ship, buoy and satellite observations (see: ecmwf.int/products/forecasts/guide/The_sea_surface_temperature_SST.html).
It is retrieved at instrument FOVs level using a 3D/4D-Var method with an error of 1 K associated with the background SST [RD 18]. The latitudes higher than 58° are excluded to avoid the presence of sea ice in the intercomparisons. The cloud filtering was based on IASI cloud test A [RD 1] and the collocated AVHRR cloud information embedded in the Day-2 IASI L1C products [RD 11].

2.2.2 Intercomparison Results

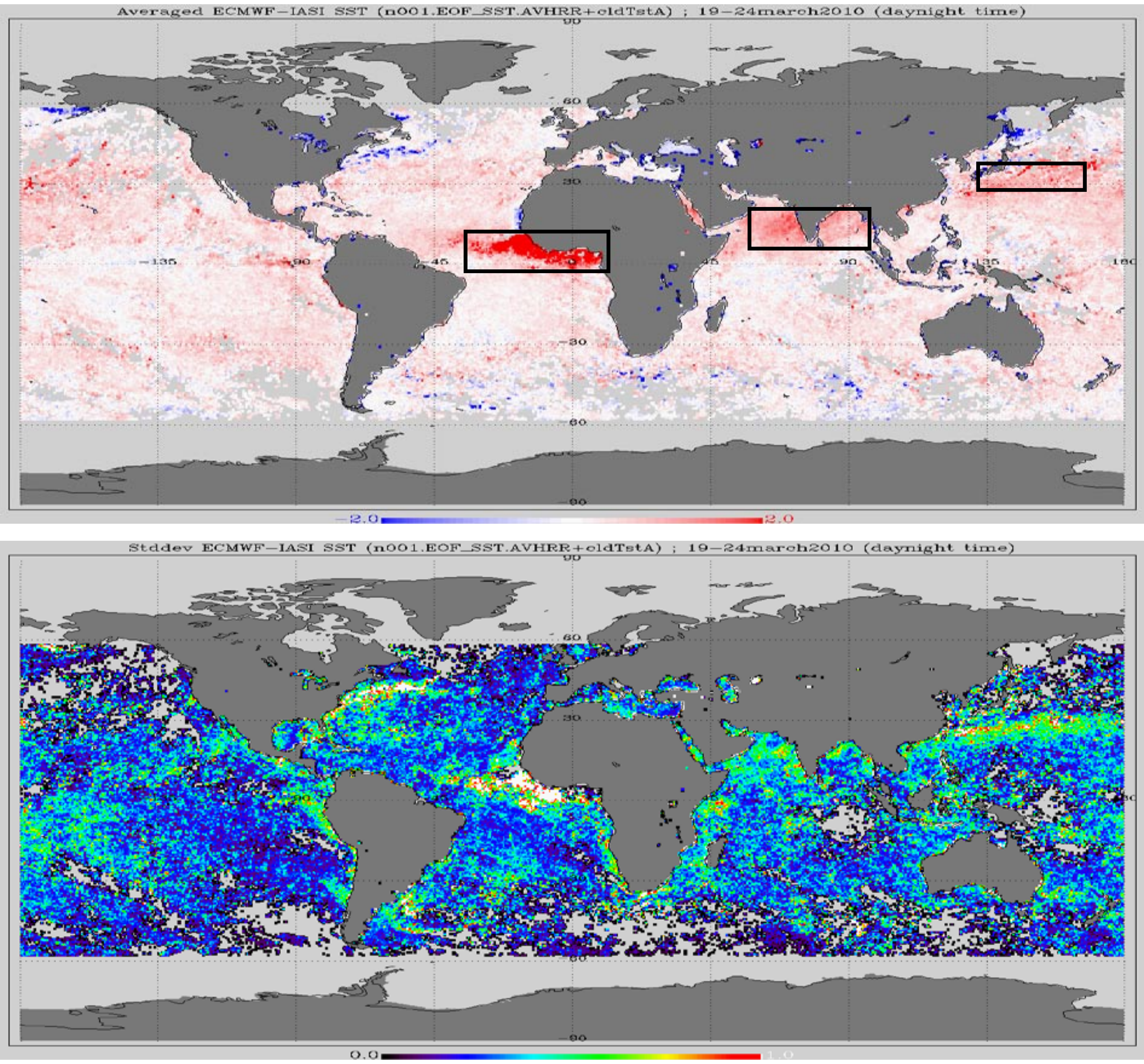

Figure 4: *(ECMWF–IASI) SST departure bias (top) and standard deviation (bottom)*

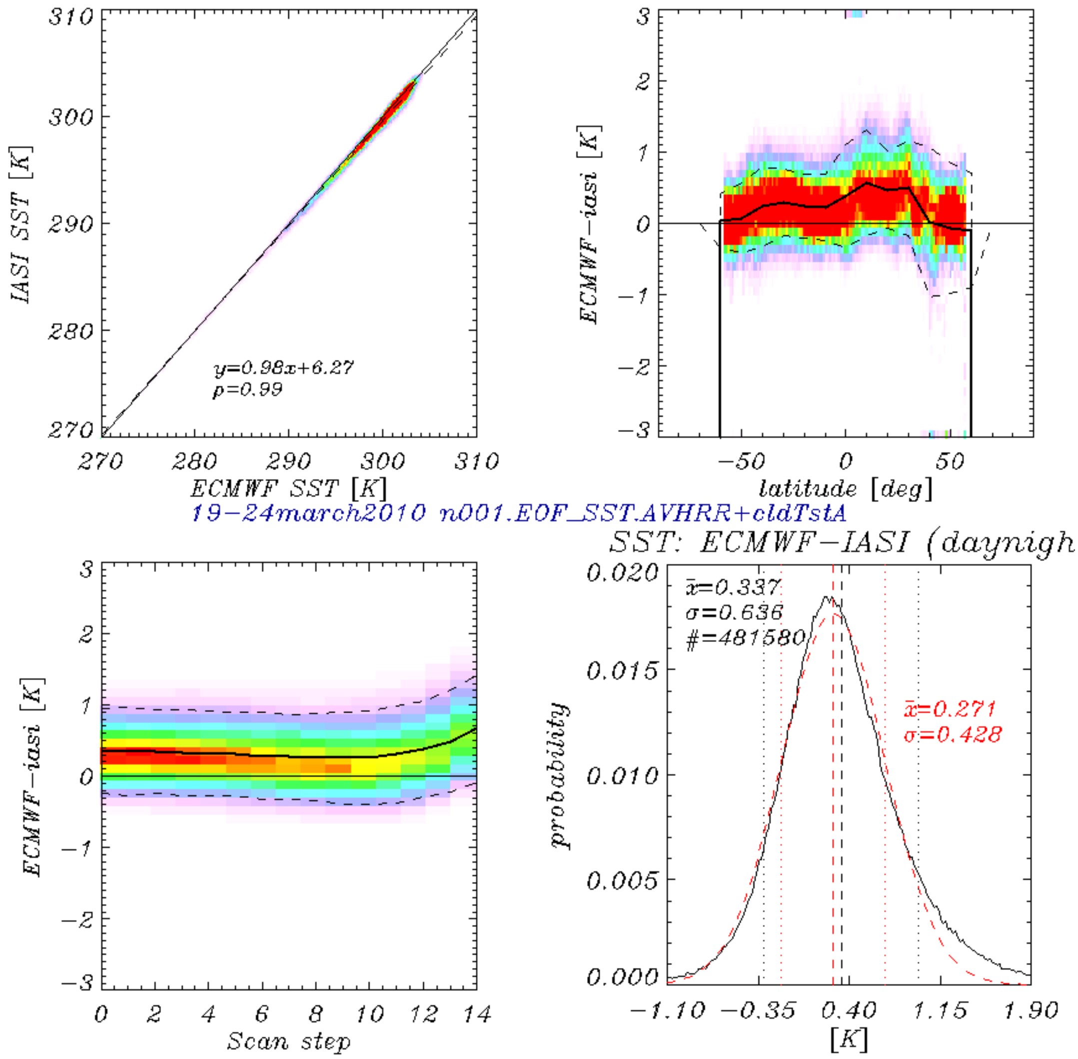

Figure 5: *(ECMWF–IASI) SST statistics for the 5-day period 19-24 March 2010. Clockwise, from upper left corner quadrant: ECMWF vs. IASI correlation, ECMWF–IASI variation with latitude, ECMWF–IASI variation with scan angle and ECMWF–IASI distribution.*

2.3 Discussion: IASI L2 Error Estimation

The statistics of the IASI SST departures from the reference products are given in Figure 3 and Figure 5. A general cold bias in IASI L2 SST is observed in both comparison studies, which amounts to about 0.44 K and 0.34 K against the AATSR and the ECMWF analysis products respectively. The overall standard deviations are of the order of 0.4 K against AATSR and 0.64 K against the model analysis. The departures show in all cases a Gaussian main mode containing at least 90% of the samples and peaking at a lower bias of 0.27 to 0.39 K, depending on the reference. The standard deviation of the main mode is also smaller and drops to 0.43 K if the reference is ECMWF and even down to 0.28 K with AATSR at night-time, when AATSR products are expected to be the most accurate. The larger errors found with ECMWF are due on the one hand to the single cloud filtering (as opposed to the double IASI PPF + AATSR match-up scheme) which, statistically, leaves more cloud-contaminated pixels, and, on the other hand, to the larger intrinsic SST errors in ECMWF in comparison to AATSR.

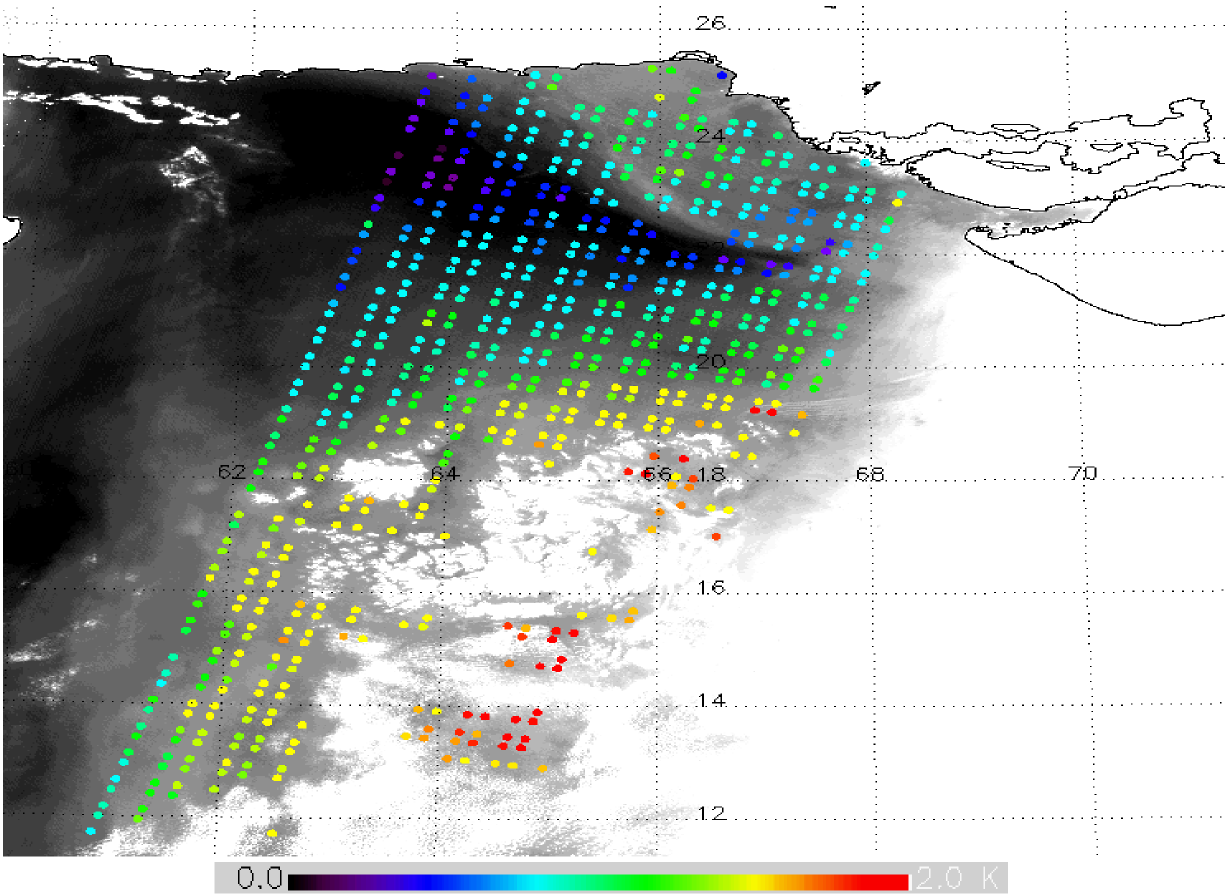

Figure 6: *(AATSR–IASI) SST plotted over an AVHRR image (visible channel) of the Arabian Sea on 19 March 2010. Land and clouds appear in saturated white, dust loads in light grey.*

A small fraction (5 to 10%) of the retrievals lies outside this main mode where IASI is systematically colder than the reference SST. The typical departures are of 1 to 1.5 K but can on rare occasions be as high as a few kelvin. This asymmetric tail is mostly attributed to undetected clouds and aerosols (dust clouds). Figure 1 & Figure 2 and Figure 4 & Figure 2 illustrate how larger departures off African coasts in the Atlantic, over the Arabian Sea and over the northern Pacific correlate with thicker aerosol optical depth as mapped with the MODIS instrument. A zoomed-in scene over the Arabian Sea is shown in Figure 6 and illustrates at a pixel level the variation of the AATSR–IASI departure with the density of the dust load.

Some statistics were recomputed after having artificially and manually excluded the areas with higher aerosol optical depths (black rectangles in Figure 1 and Figure 4). The results are given in Figure 7, where the global bias drops down below 0.3 K. It becomes as low as 0.23 K if comparisons are made to ECMWF. The standard deviation of (reference–IASI) differences for such dust-clear pixels is also much smaller, 0.28 K against AATSR and 0.55 K against ECMWF. The current operational implementation does however not run such tests as can identify or filter out the dust-contaminated pixels. These figures, although still theoretical as long as aerosols are not effectively detected, can be extrapolated to the sea areas which are climatologically clean of dust.

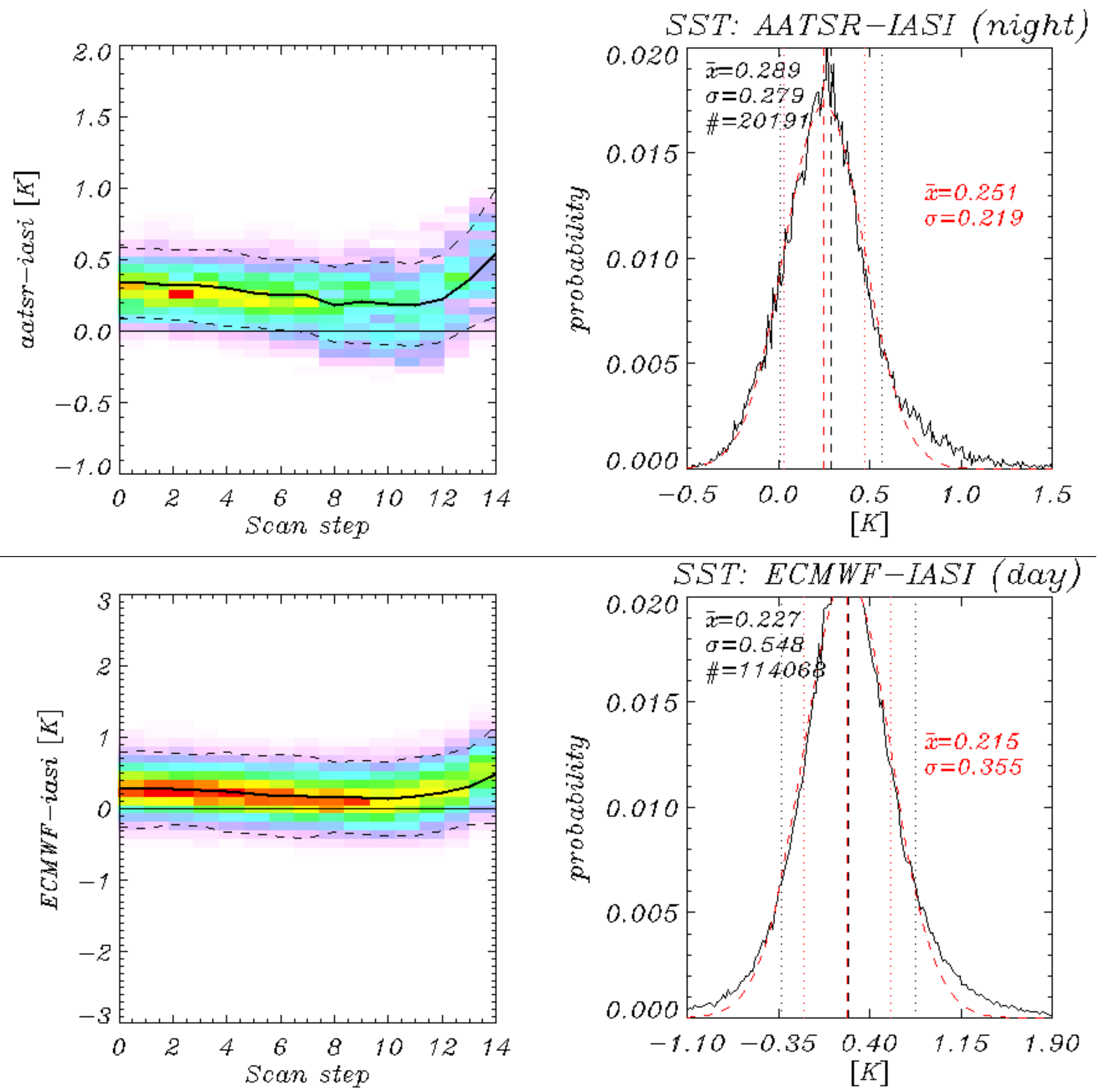

Figure 7: *IASI SST departures from AATSR (top) and ECMWF (bottom) between 19 and 24 March 2010 excluding the dusty areas in the Atlantic, the Arabian Sea and the Northern Pacific*

Eventually, regardless of the dust filtering, the choice of the reference products and the illumination of the scene, the IASI SST retrievals show a consistent variation with the scan angle of about 0.3 K from the nadir to the swath edge. Further algorithmic developments, explicitly taking into account the geometry in the retrievals, are ongoing to correct for this effect.

2.4 Validation with In-situ Measurements (Buoys) and Satellite Data (AVHRR/Metop and SEVIRI/Meteosat)

A systematic validation including comparisons with drifting buoys SSTs as well as a three-way error analyses with AVHRR and SEVIRI SST (L3) products has been running to characterise the quality of the IASI L2 SST retrievals [RD 13]. The study supports the generation of IASI SST L2P products as defined by the Group for High Resolution Sea

Surface Temperature (GHRSST) [http://www.ghrsst.org]. This document may be referred to for an exhaustive description of the analysis, of which the main validation and intercomparison results are summarised hereafter. They confirm an error standard deviation of approximately 0.4 K and a systematic cold bias of the same order, which is consistent with the studies presented in the previous sections.

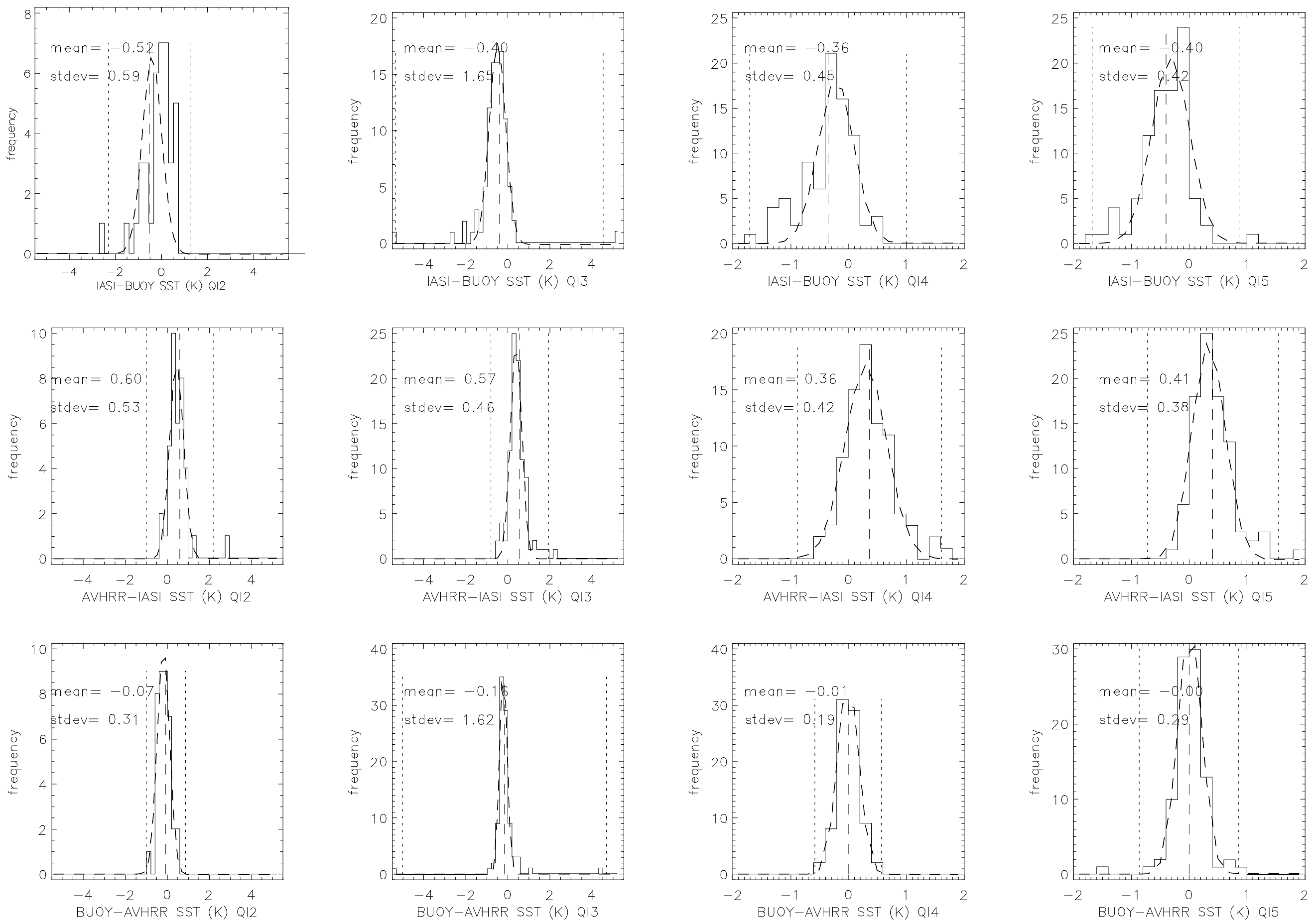

Figure 8: *SST comparisons between IASI and buoys (top row), AVHRR and IASI (middle) and buoys and AVHRR (bottom) for four product quality classes: 2 (weakest) to 5 (best) from left to right, 1-30 November 2008*

3 LAND SURFACE TEMPERATURE

3.1 Comparison with SEVIRI LST LSA-SAF Products

3.1.1 Data Description and Match-up Criteria

The Land Surface Analysis (LSA) Satellite Application Facility (SAF) generates an operational LST product based on the Spinning Enhanced Visible and Infrared Imager (SEVIRI) measurements acquired from the Meteosat Second Generation (MSG) satellites. The retrieved physical parameter is the radiative skin temperature over land and is available under clear sky conditions only. Derived from thermal infrared measurements, it is directly comparable in nature to the IASI LST. Its computation involves a generic split window (GSW) algorithm [RD 14] with two adjacent window channels – IR10.8 and IR12.0 µm – to correct for the atmospheric absorption. The spatial resolution is that of the SEVIRI images in a nominal mode, of approximately 3 km at the sub-satellite point, with a coverage including the whole of Europe, all of Africa and a portion of South America (see Figure 9).

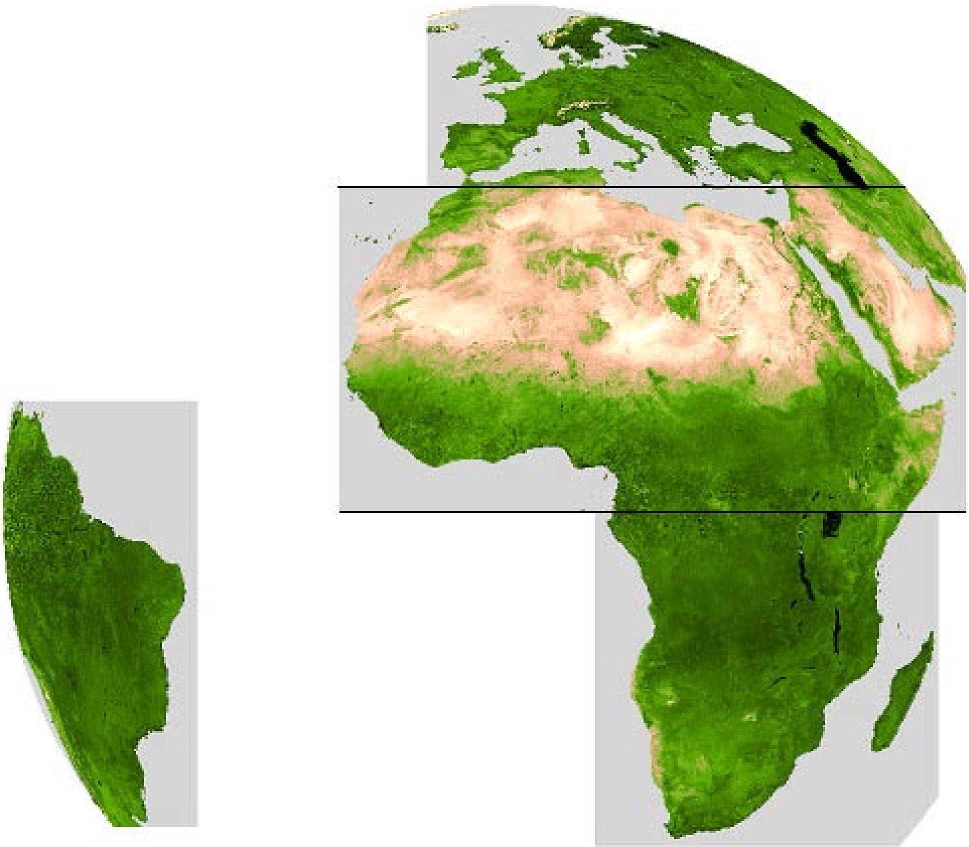

Figure 9: *The LSA SAF geographical areas*

The periodicity of these products is 15 minutes which allows a very close temporal coincidence with the successive Metop overpasses and their associated IASI LST retrievals. Each LSA LST comes with a quality flag [RD 16] indicating the degree of confidence and the error associated with the retrieval. For this study, we only retained the products with “above nominal” and “nominal” quality for both the LST and surface emissivity parameters. This corresponds to uncertainties of less than 1 K and between 1 and 2 K respectively [RD 15 and http://landsaf.meteo.pt/algorithms.jsp?seltab=0&starttab=0#uncertainties].

The LST retrievals in the IASI L2 PPF v5 are the result of an optimal estimation method using climatological *a priori* information which is initialised with a statistical retrieval, namely an EOF regression [RD 17]. The latter method differs from the one implemented in the former versions of the IASI L2 PPF and which used to directly form the final L2 products. It will be referred to as FG (first guess) or as DZ in the rest of the document, after its author's initials (Dan Zhou, NASA). The main conceptual difference is the explicit tuning of the retrieval to the viewing geometry, achieved with dedicated coefficients for various satellite zenith angles. Because of these changes and in order to characterise the impact of the modifications and the improvements resulting from the PPF upgrade, all three retrievals were applied to the same data set and compared to the same reference products. The common data set consists of a 6-day period from 19 to 24 March 2010. As for the cloud filtering, likewise described in the SST section, it relied on a IASI stand-alone algorithm in version 4 which is complemented with the AVHRR cloud mask in version 5. In addition, a third test had to be used in the experiment running the DZ LST retrieval which assesses the optical thickness from the IASI principal spectral components [RD 17]. Depending on the optical thickness, the scene is declared fully clear or cloud contaminated and different coefficients are used for the atmospheric parameters first-guess retrieval. Fully clear IFOVs are considered here. On average, 90% of the clear sky situations identified by the IASI cloud test A and the AVHRR cloud mask are consistently confirmed by this method.

Departures (LSA SAF *minus* IASI) were computed for each match-up where at least four good LSA LST retrievals could be found within the IASI field of view. The matching SEVIRI points were averaged and only used if their standard deviations remained lower than 5 K to avoid too-heterogeneous scenes. The intercomparisons were performed for day- and night-times separately. Under Sun illuminations, differences are indeed expected due to shadow effects coming from the relative Metop/MSG – Sun – Surface geometry. The statistics were computed globally with the exclusion of the Sahara, where the PPF v4 LST retrievals during daytime in particular present too-large variances. The African Sahara and the Arabian Peninsula were then isolated and the statistics specifically repeated for these unique soil types.

3.1.2 LSA SAF – PPF v5 (OEM), 19-24 March 2010

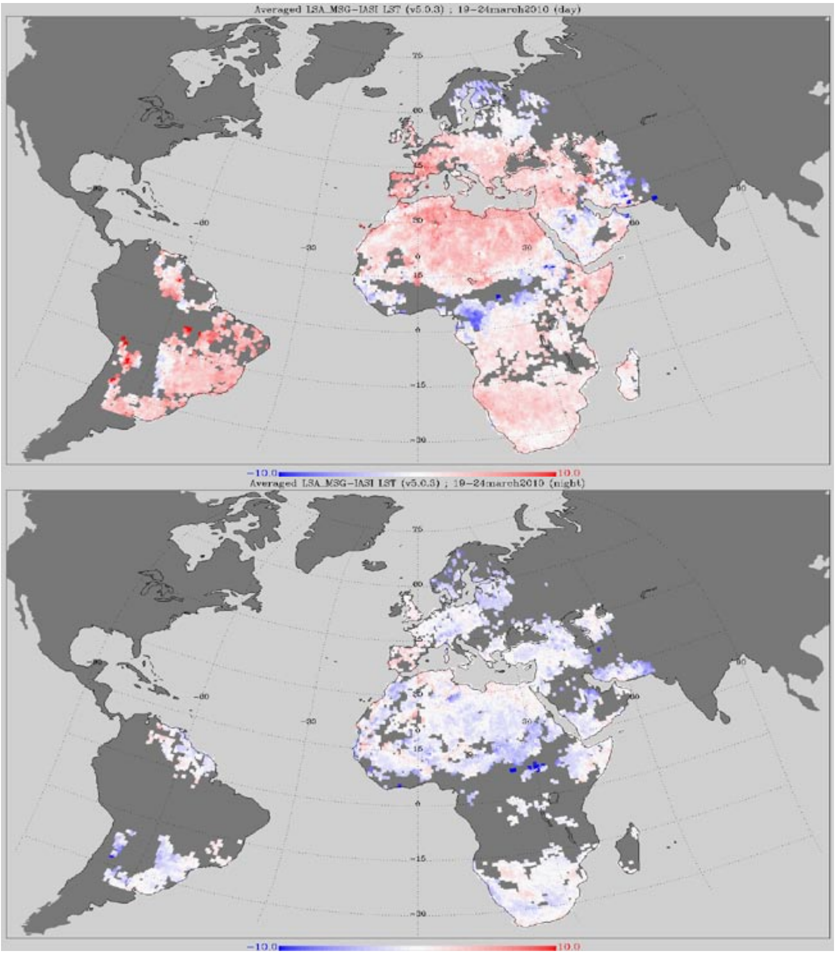

Figure 10: *Mean departures for day (top) and night (bottom)*

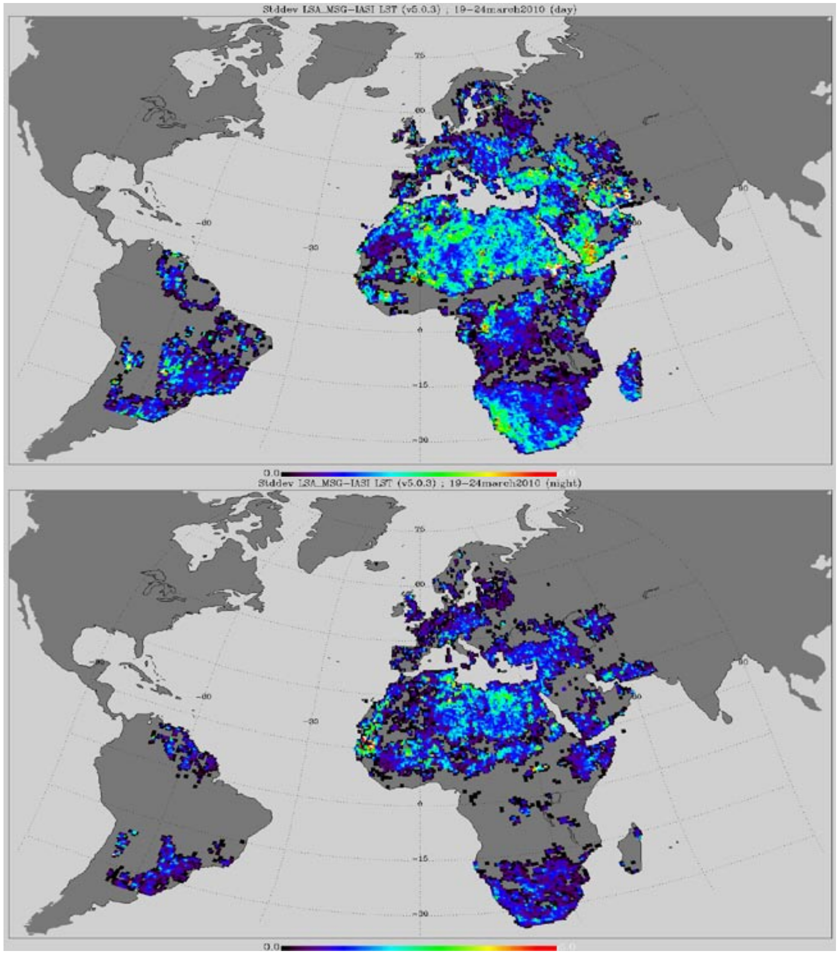

Figure 11: *Error standard deviations for day (top) and night (bottom)*

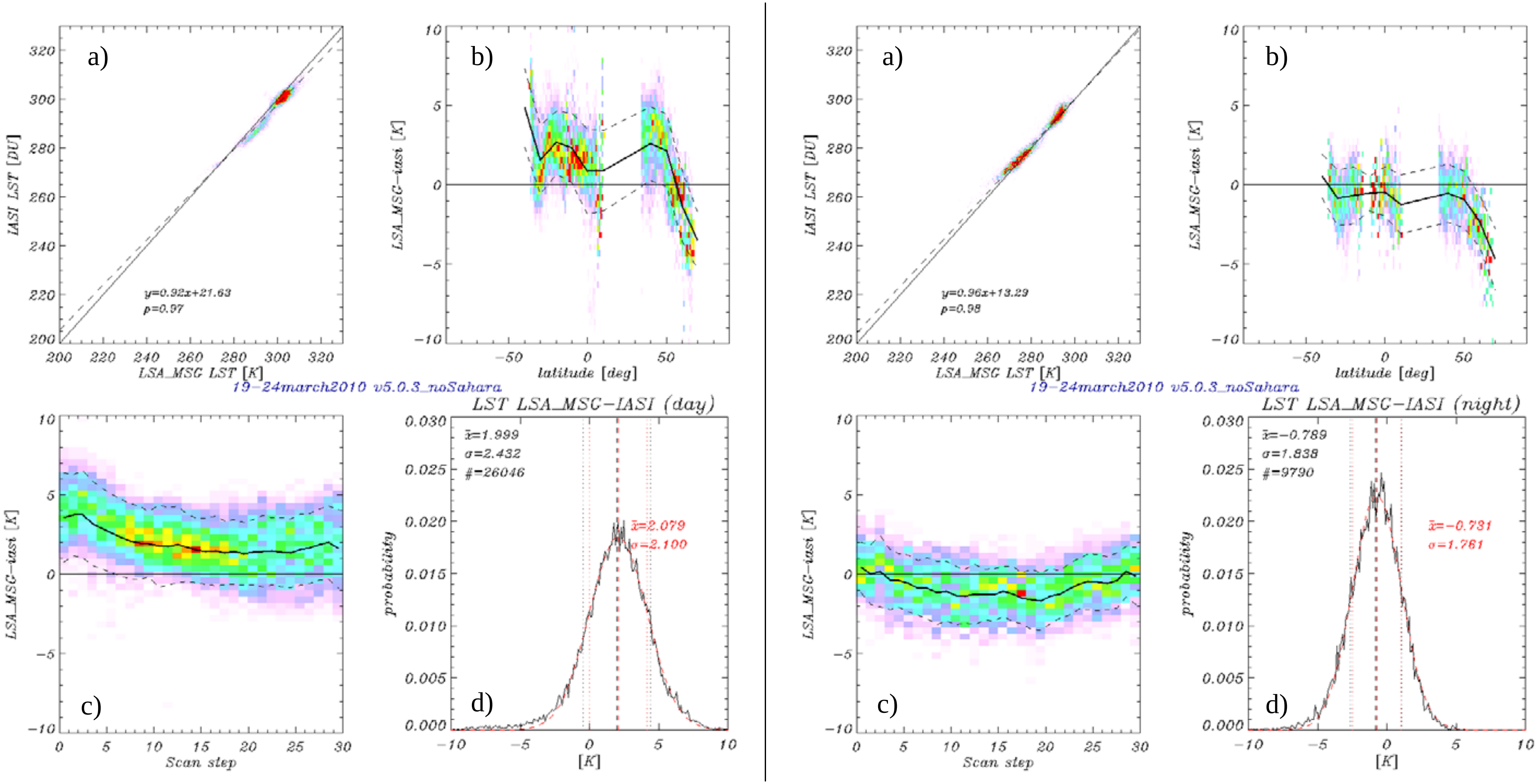

Figure 12: *Correlation (a) and statistics (d) of LSA SAF – IASI (PPF v5 OEM) LST departures and their variations with latitude (b) and scan angle (c) for day- and night-times (left and right panels, respectively) for all regions, Sahara excluded*

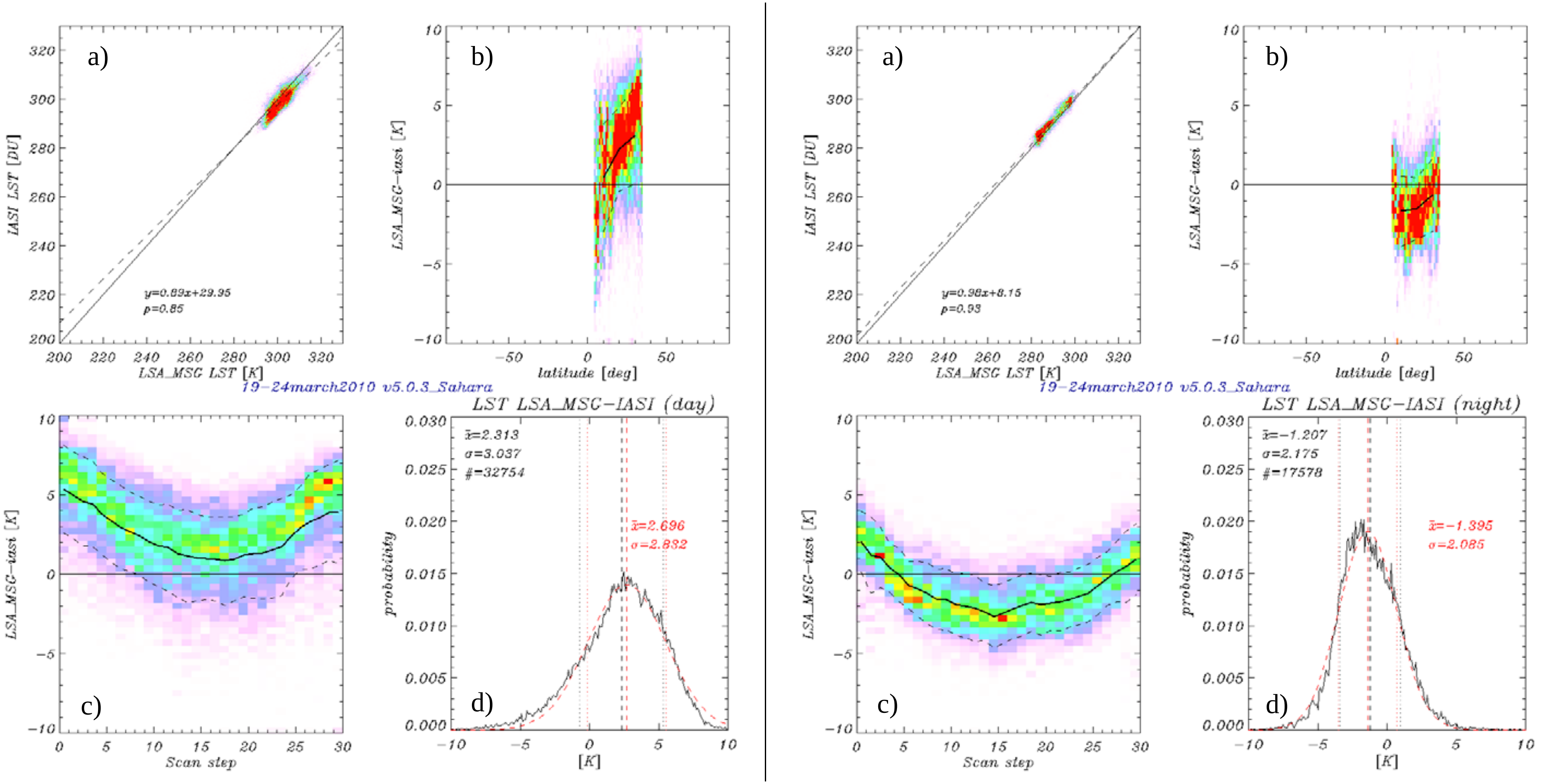

Figure 13: *Same as* ***Figure 12****, for the Sahara only*

3.1.3 LSA SAF – PPF v5 (FG), 19-24 March 2010

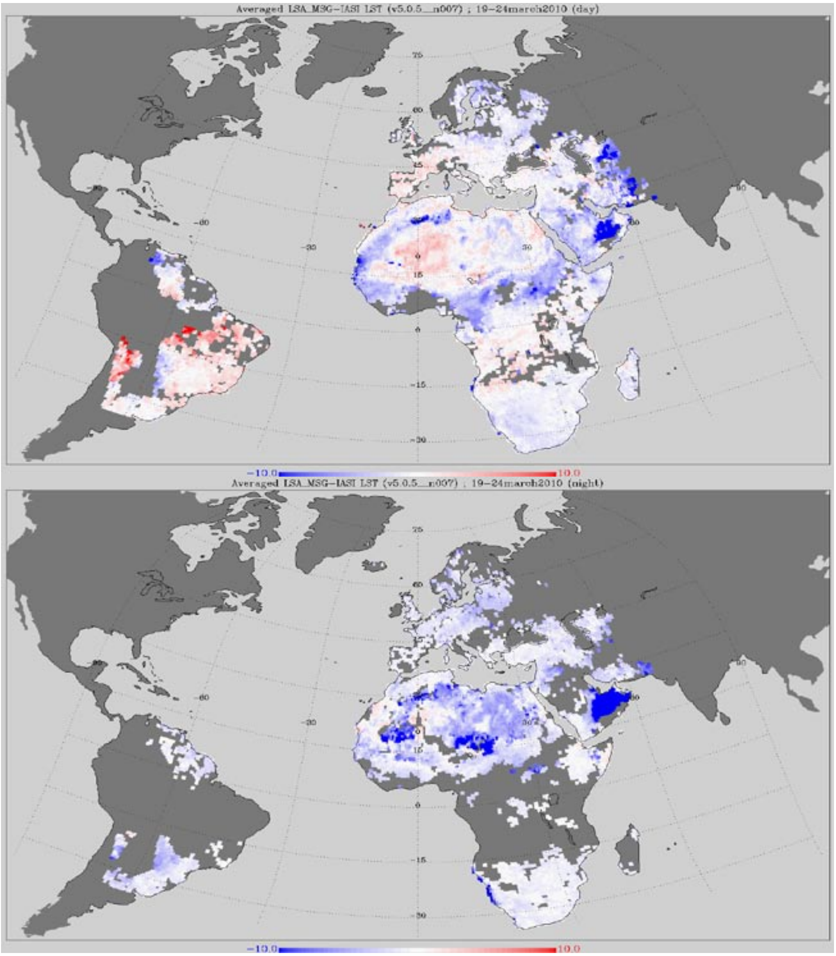

Figure 14: *Mean departures for day (top) and night (bottom)*

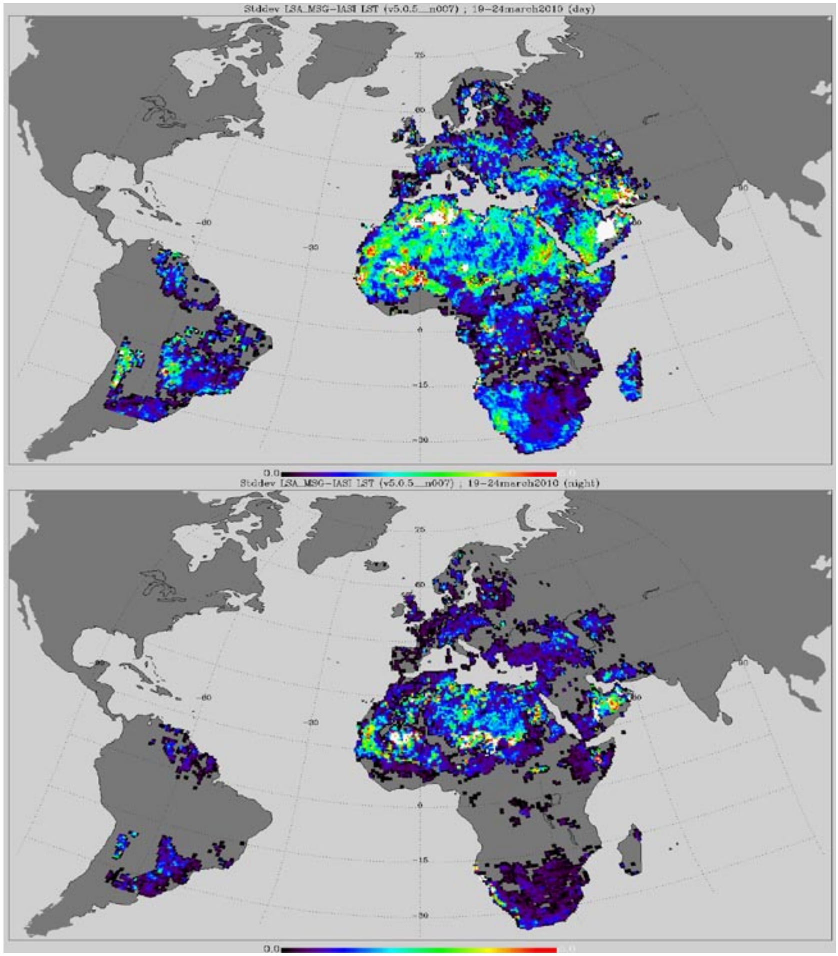

Figure 15: *Error standard deviations for day (top) and night (bottom)*

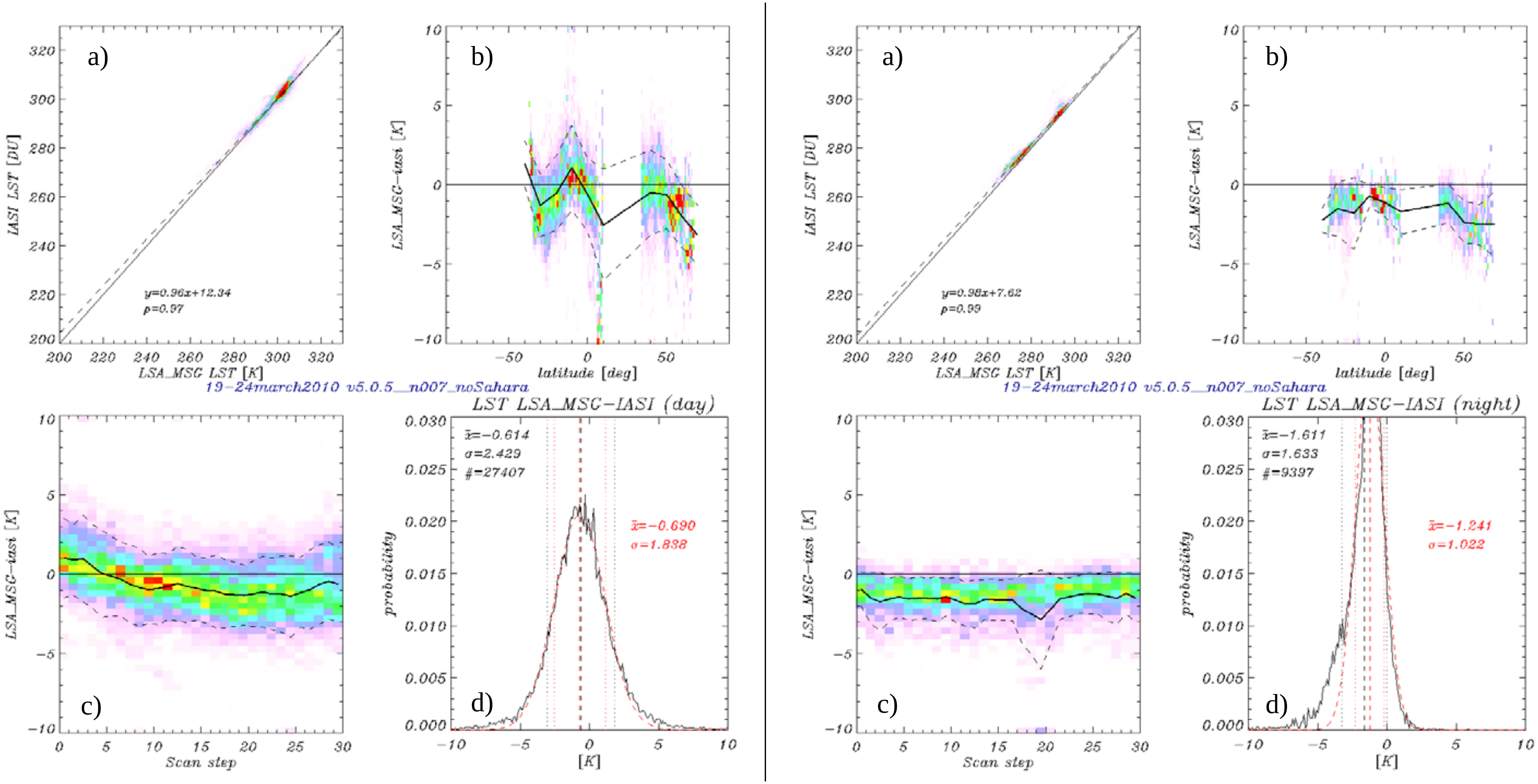

Figure 16: *Correlation (a) and statistics (d) of LSA SAF – IASI (PPF v5 FG) LST departures and their variations with latitude (b) and scan angle (c) for day- and night-times (left and right panels, respectively) for all regions, Sahara excluded*

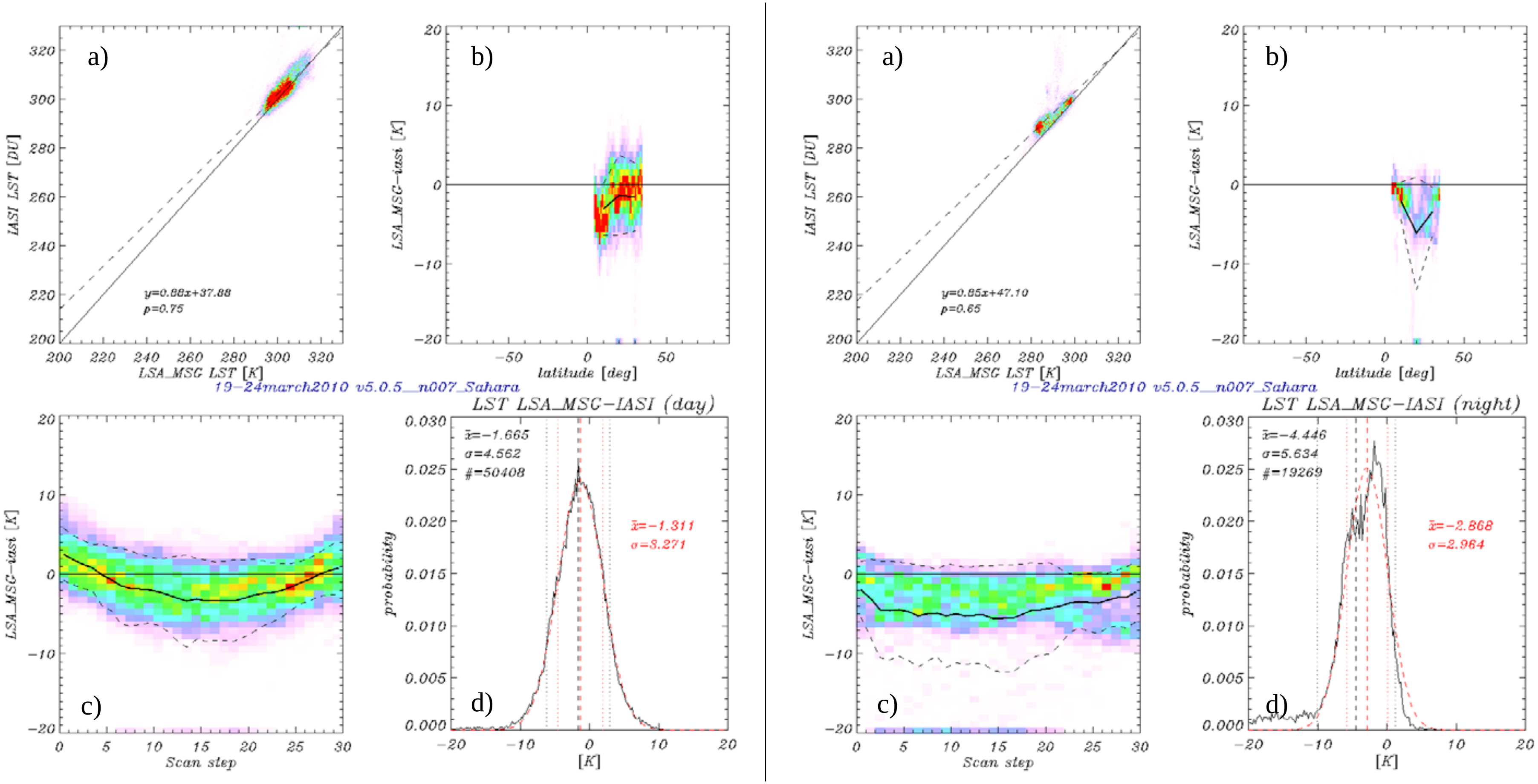

Figure 17: *Same as **Figure 16**, for the Sahara only*

3.1.4 LSA SAF – PPF v4.3, 19-24 March 2010

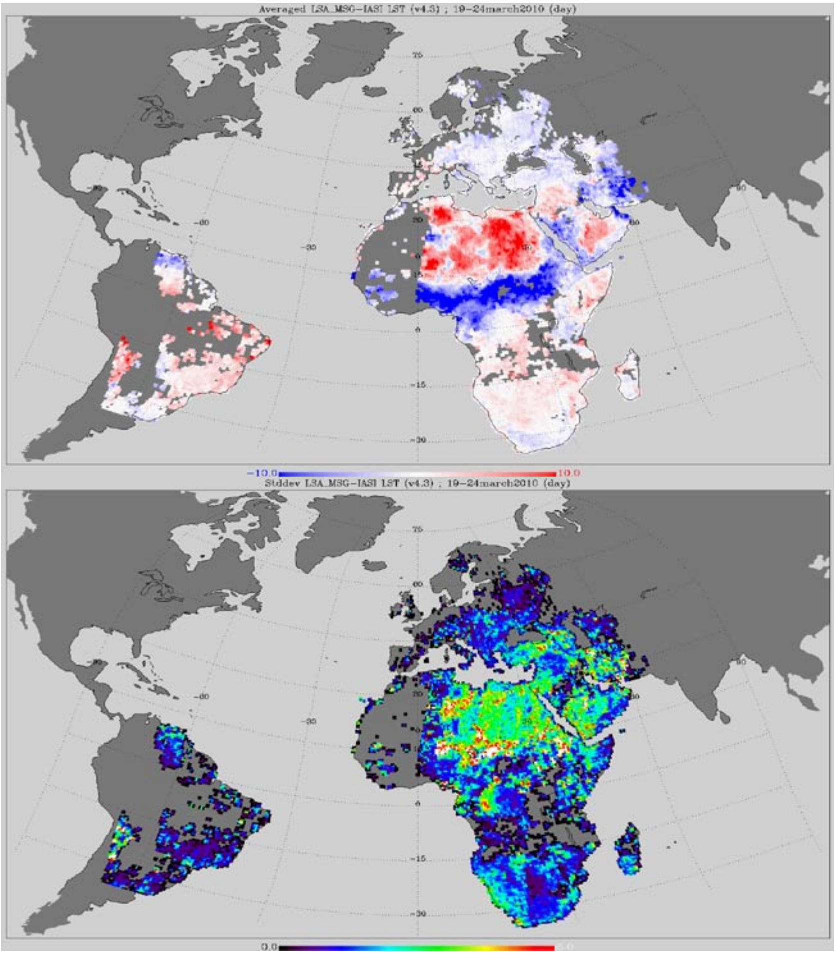

Figure 18: *Mean departures for day (top) and night (bottom)*

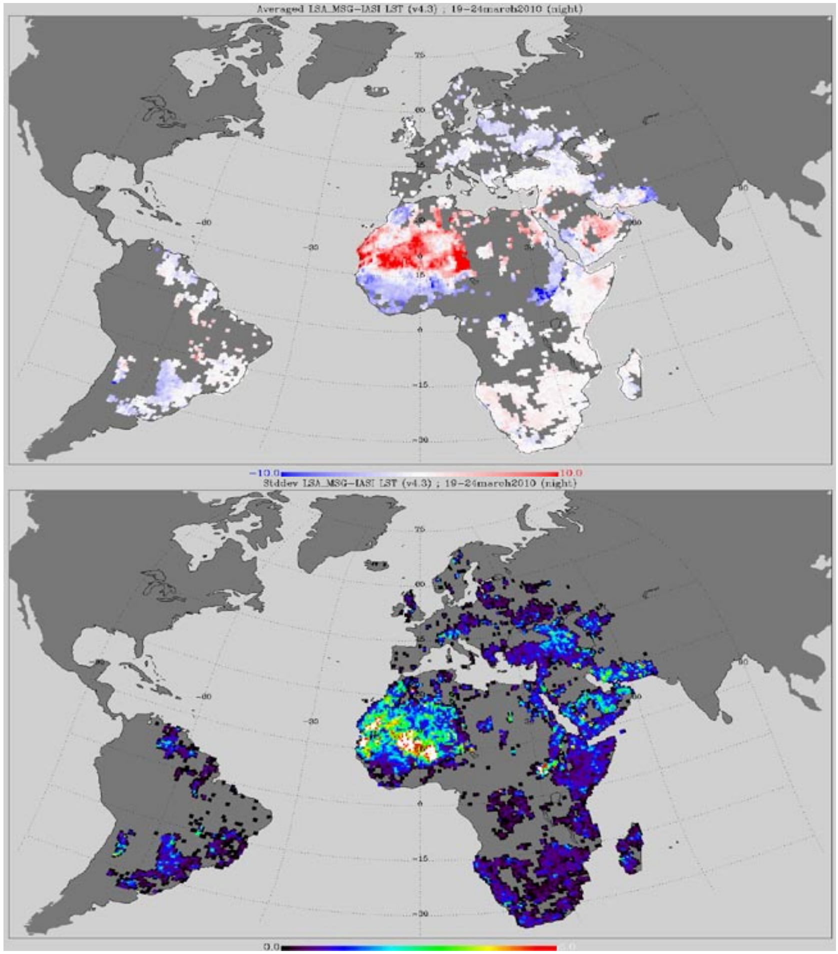

Figure 19: *Error standard deviations for day (top) and night (bottom)*

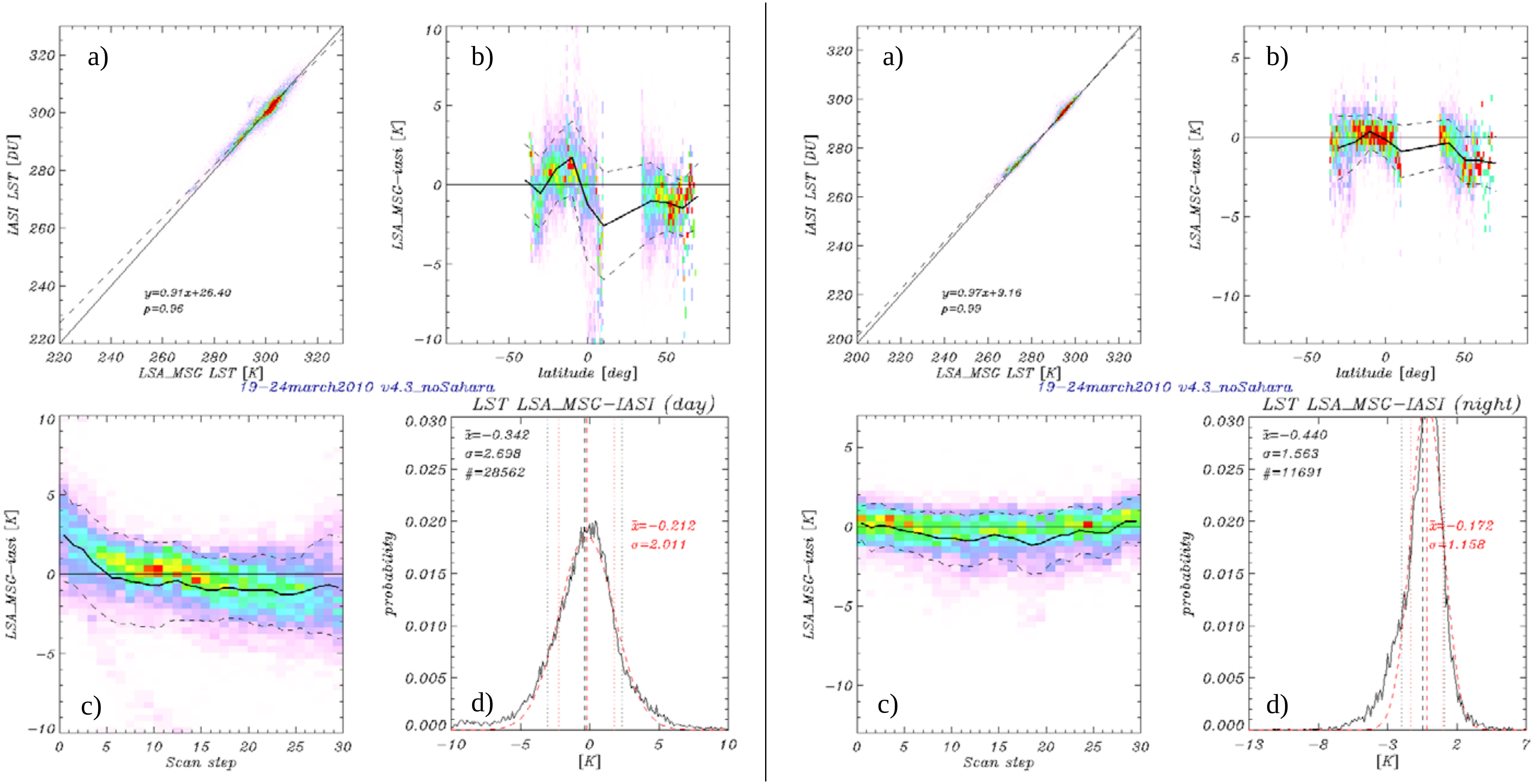

Figure 20: *Correlation (a) and statistics (d) of LSA SAF – IASI (PPF v4) LST departures and their variations with latitude (b) and scan angle (c) for day- and night-times (left and right panels, respectively) for all regions, Sahara excluded*

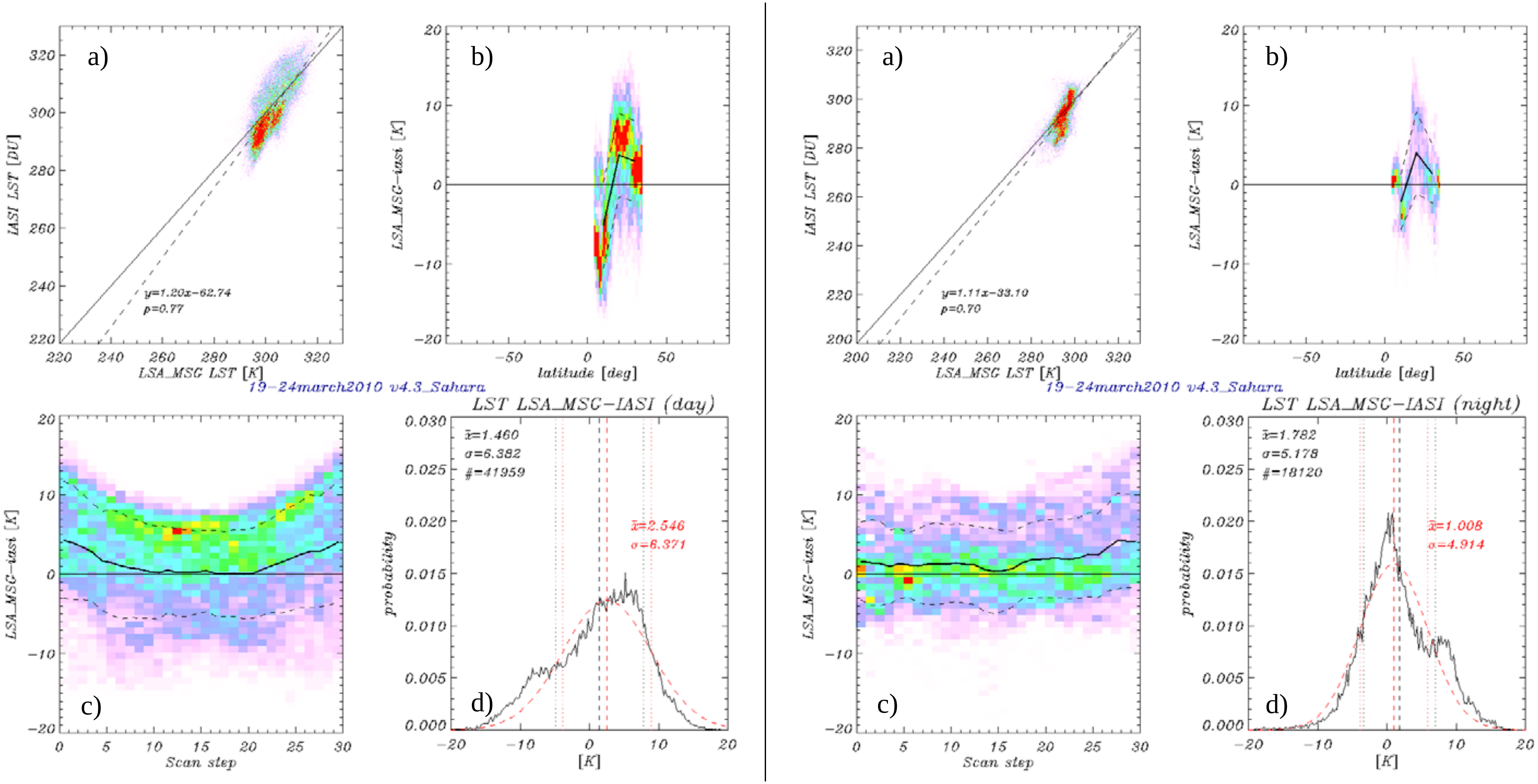

Figure 21: *Same as* ***Figure 20****, for the Sahara only*

3.2 Comparison with ECMWF Analyses

3.2.1 Data Description and Match-up Criteria

The intercomparison results presented and discussed in the previous section are limited to the portion of the Earth accessible to MSG-2 instruments. A systematic comparison of the IASI LST with ECMWF analyses was therefore carried out to infer a more global characterisation of the retrieval performances. The ECMWF analysis surface temperatures are available with a 6-hour temporal resolution on a 0.5°x0.5° spatial grid. They derive from the assimilation of IR and microwave sensors and instrument measurements, and are based on a 3D/4D variational retrieval which associates an error of 5 K to the LST [RD 18].

Each IASI IFOV was matched to its nearest neighbour in the ECMWF grid after a temporal interpolation of the modelled LST to the acquisition time. Clear sky situations only were retained in this study which focused on the 19-24 March 2010 period. The respective cloud filtering of the versions v4, v5 OEM and v5 FG is the same as described in Section 3.1.1 for comparisons against LSA SAF products. Global statistics excluding latitudes higher than 60°, as well as surfaces above 2000 m and the Sahara, are presented first. Specific statistics for the Sahara and the polar caps were then computed in turn and the respective intercomparison results are presented hereafter.

3.2.2 ECMWF – PPF v5 (OEM), 19-24 March 2010

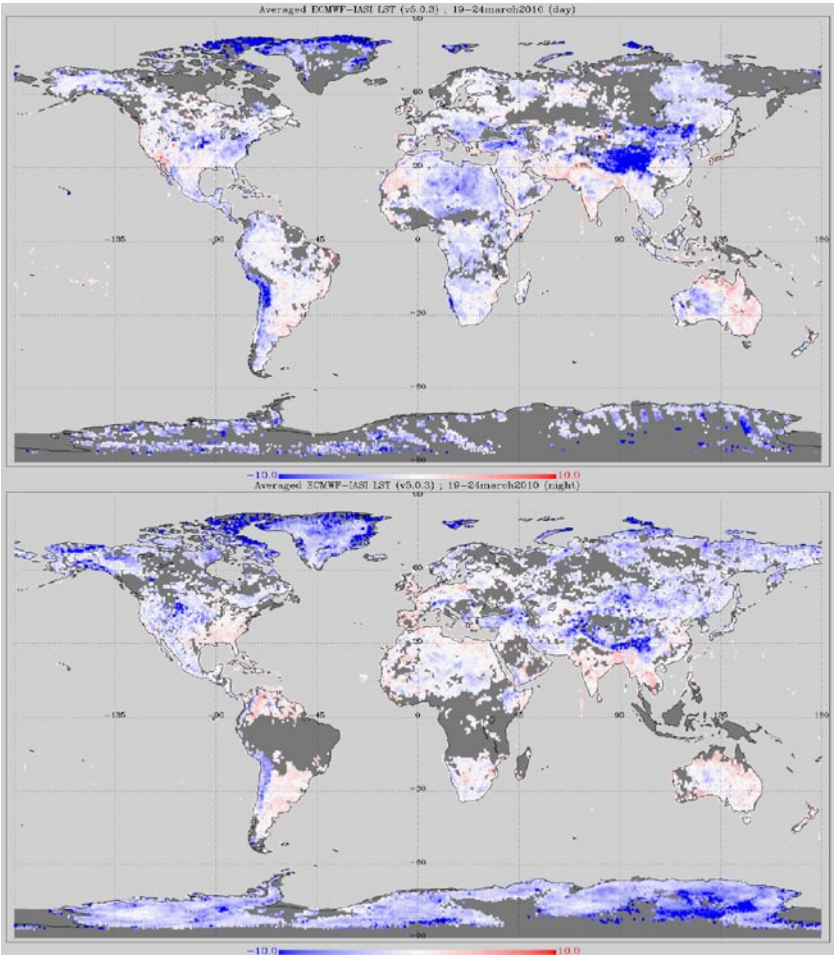

Figure 22: *Mean departures for day (top) and night (bottom)*

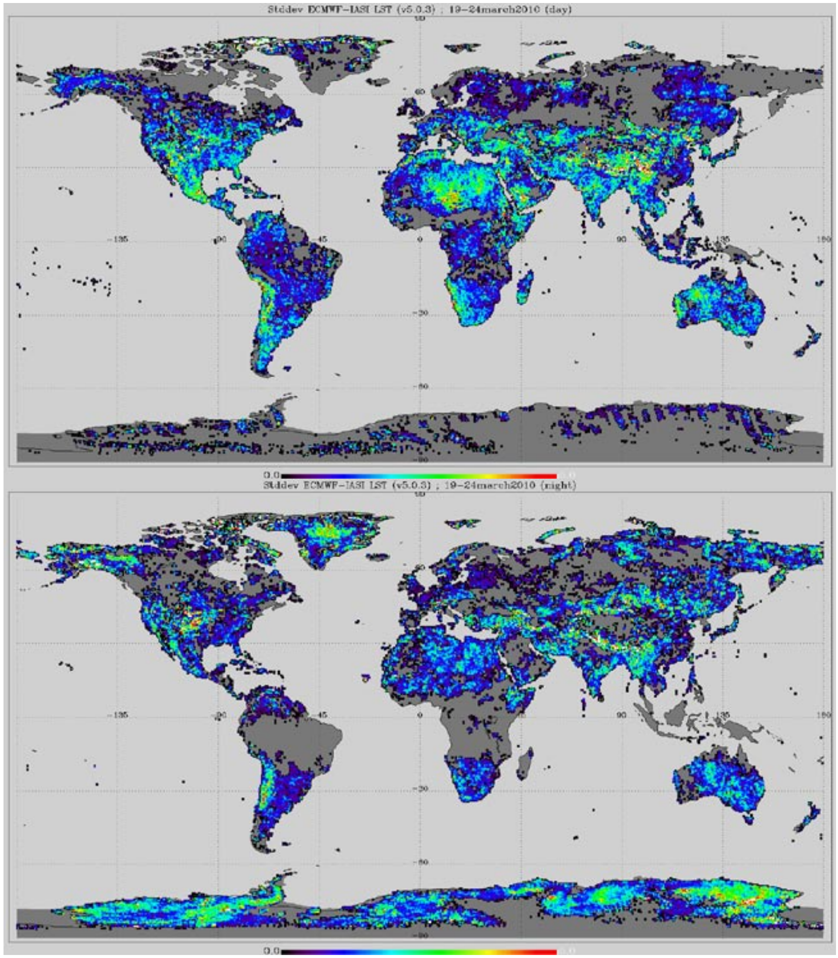

Figure 23: *Error standard deviations for day (top) and night (bottom)*

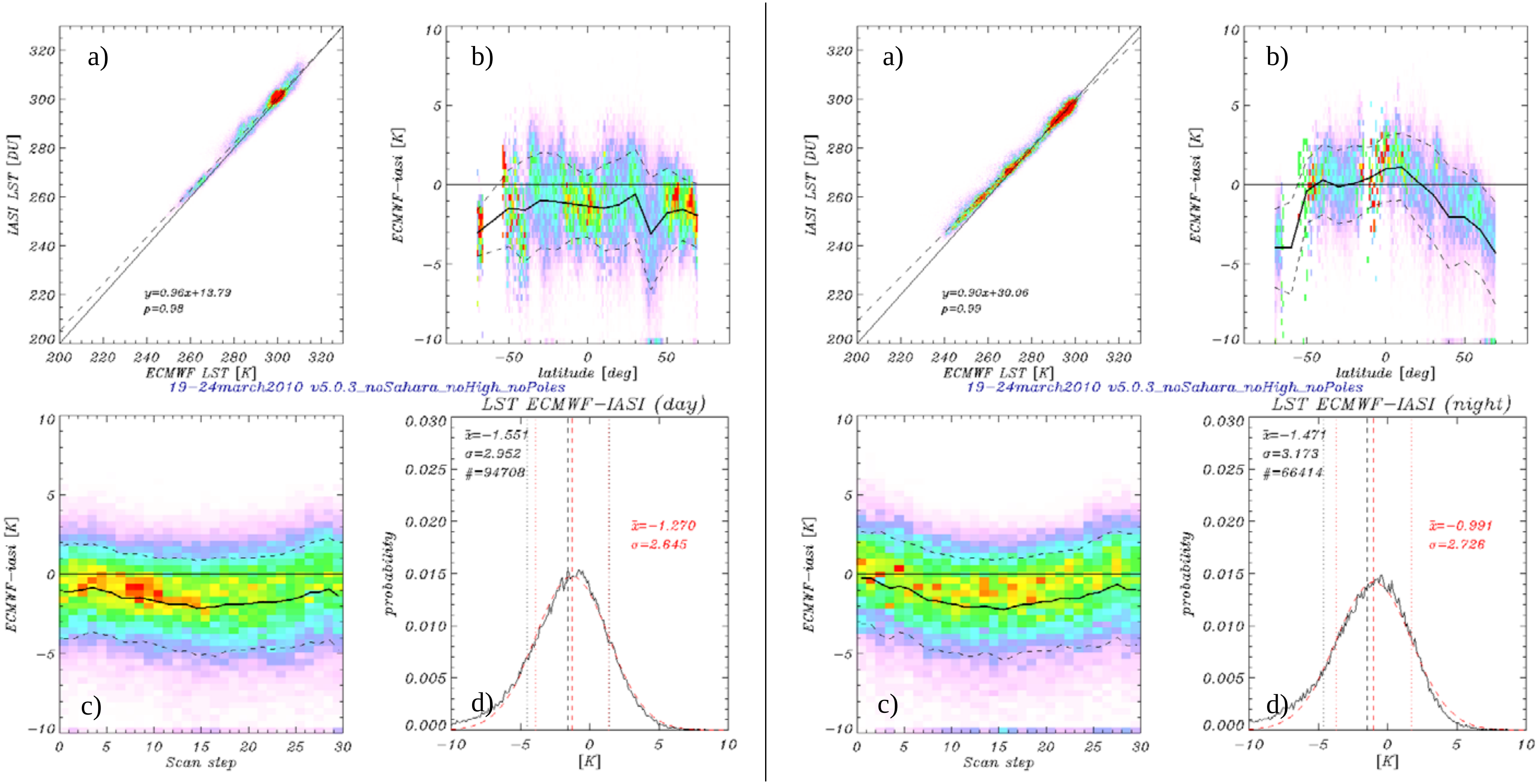

Figure 24: *Correlation (a) and statistics (d) of ECMWF – IASI (PPF v5 OEM) LST departures and their variations with latitude (b) and scan angle (c) for day- and night-times (left and right panels, respectively). Sahara, polar and elevated regions (Ps<800 hPa) were excluded.*

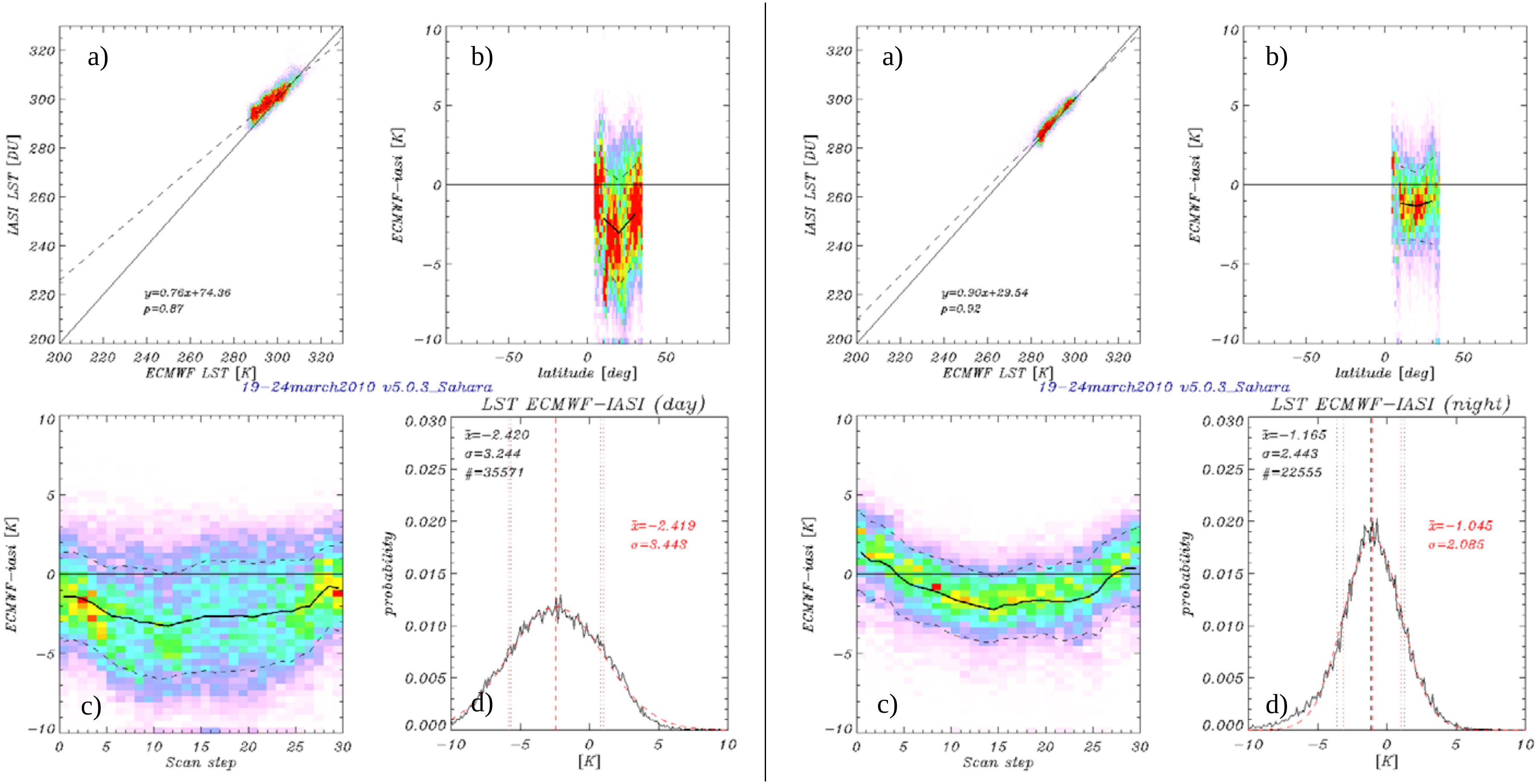

Figure 25: *Same as* ***Figure 24****, for the Sahara only*

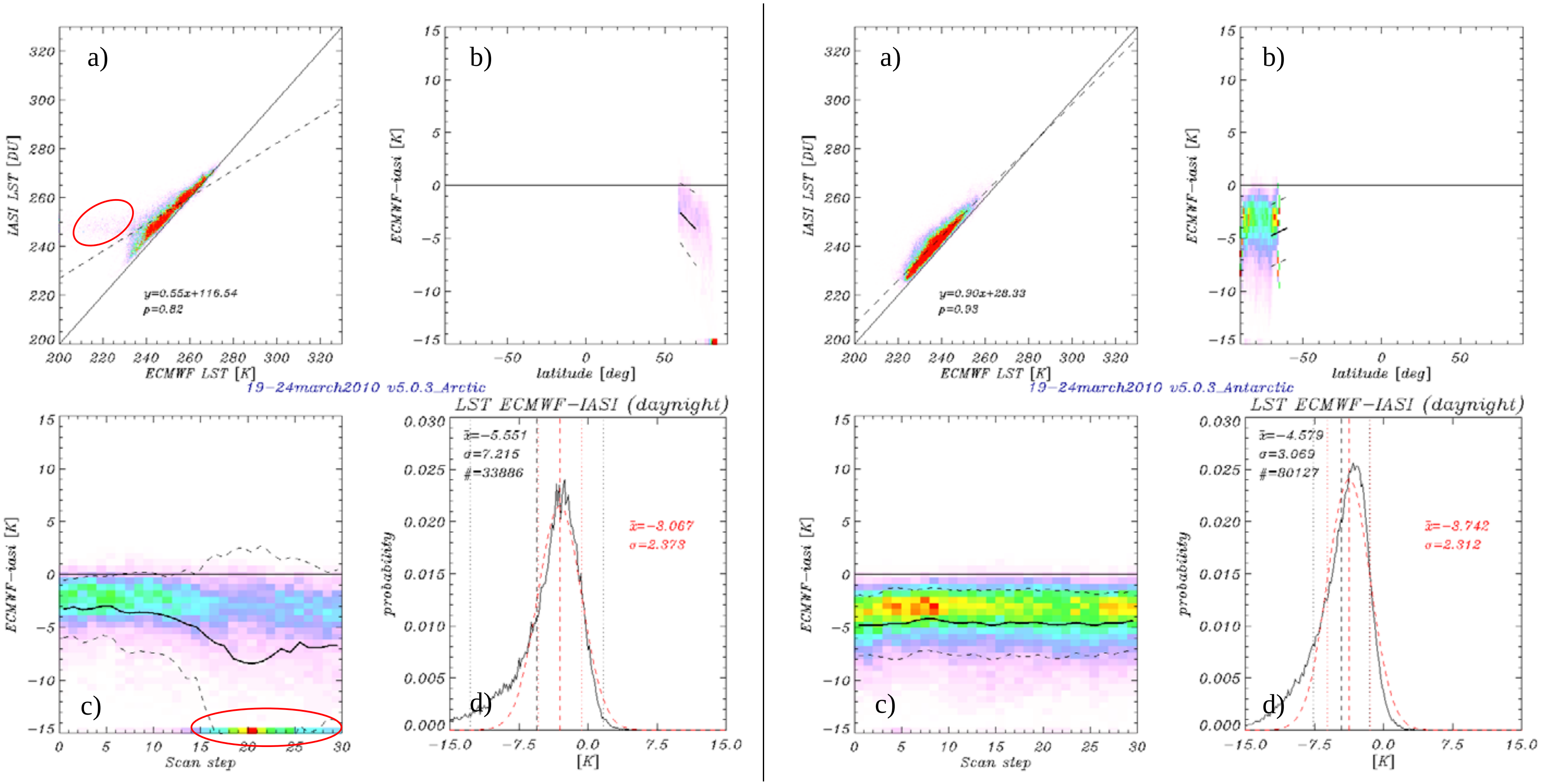

Figure 26: *Same as* ***Figure 24****, for the Arctic (left) and Antarctica (right)*

3.2.3 ECMWF – PPF v5 (FG), 19-24 March 2010

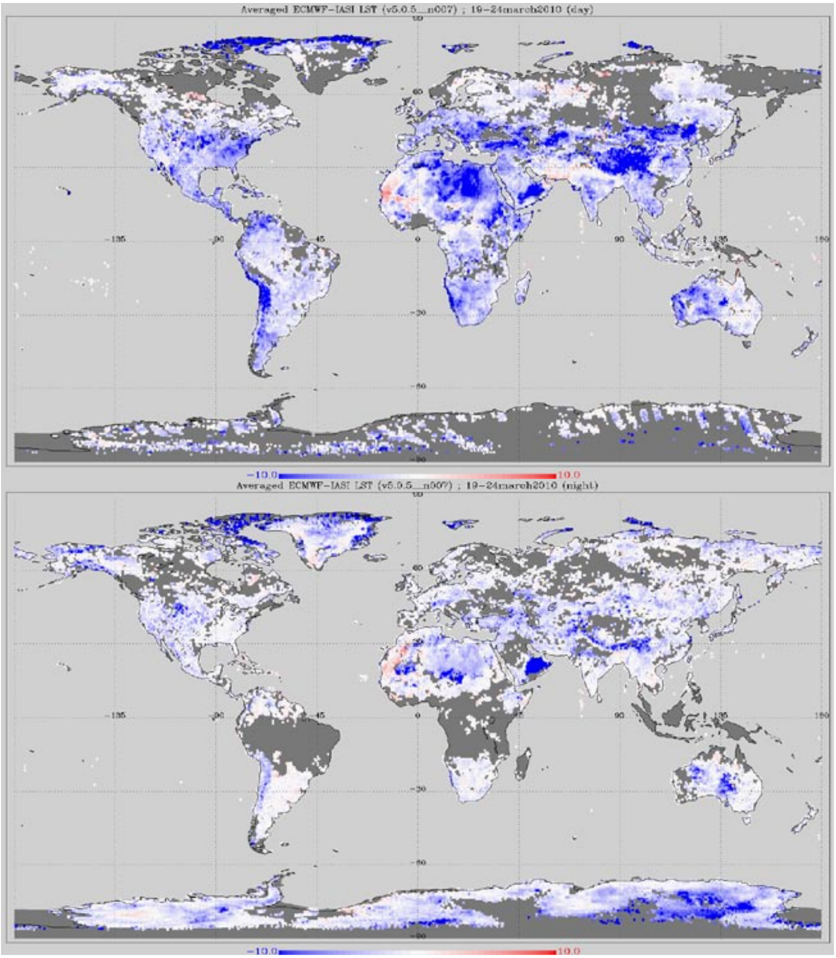

Figure 27: *Mean departures for day (top) and night (bottom)*

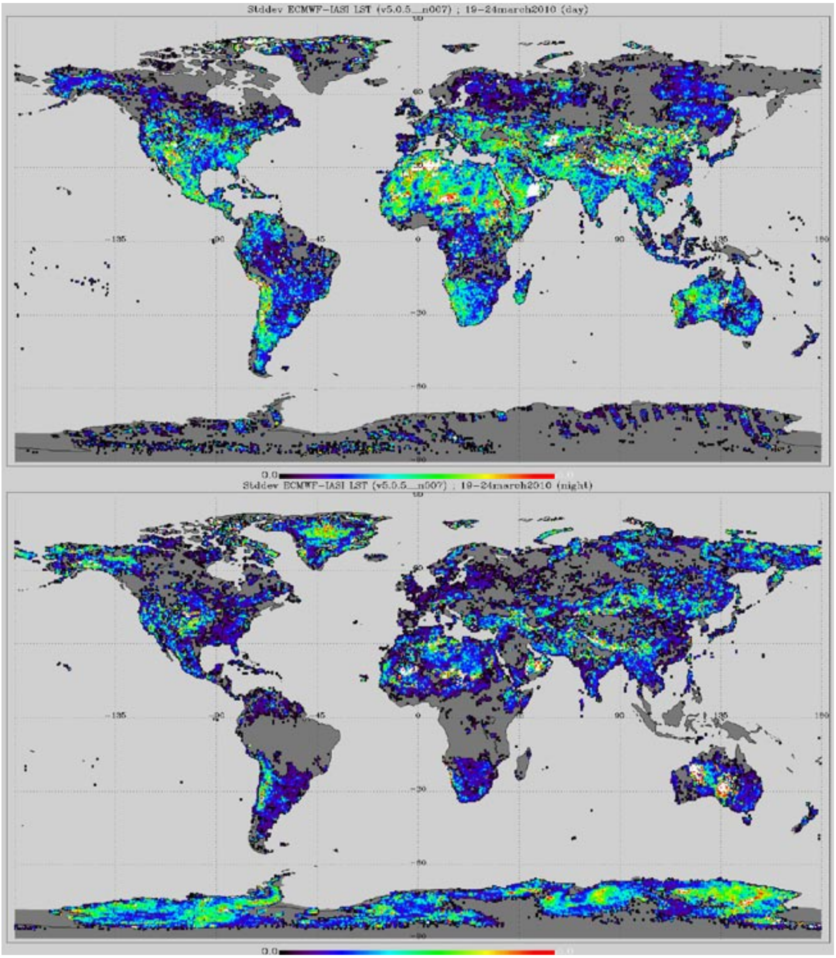

Figure 28: *Error standard deviations for day (top) and night (bottom)*

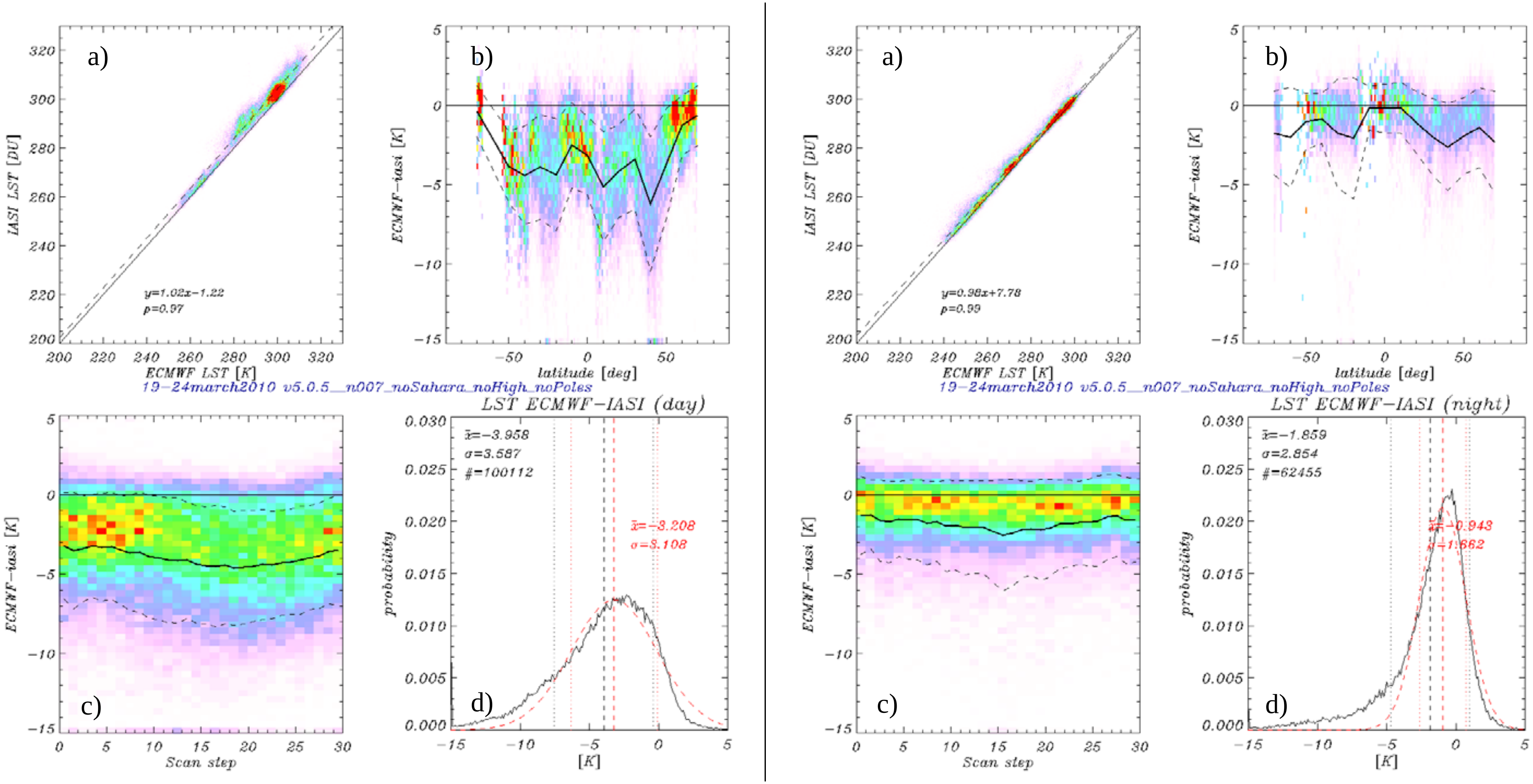

Figure 29: *Correlation (a) and statistics (d) of ECMWF – IASI (PPF v5 FG) LST departures and their variations with latitude (b) and scan angle (c) for day- and night-times (left and right panels, respectively). Sahara, polar and elevated regions (Ps<800 hPa) were excluded.*

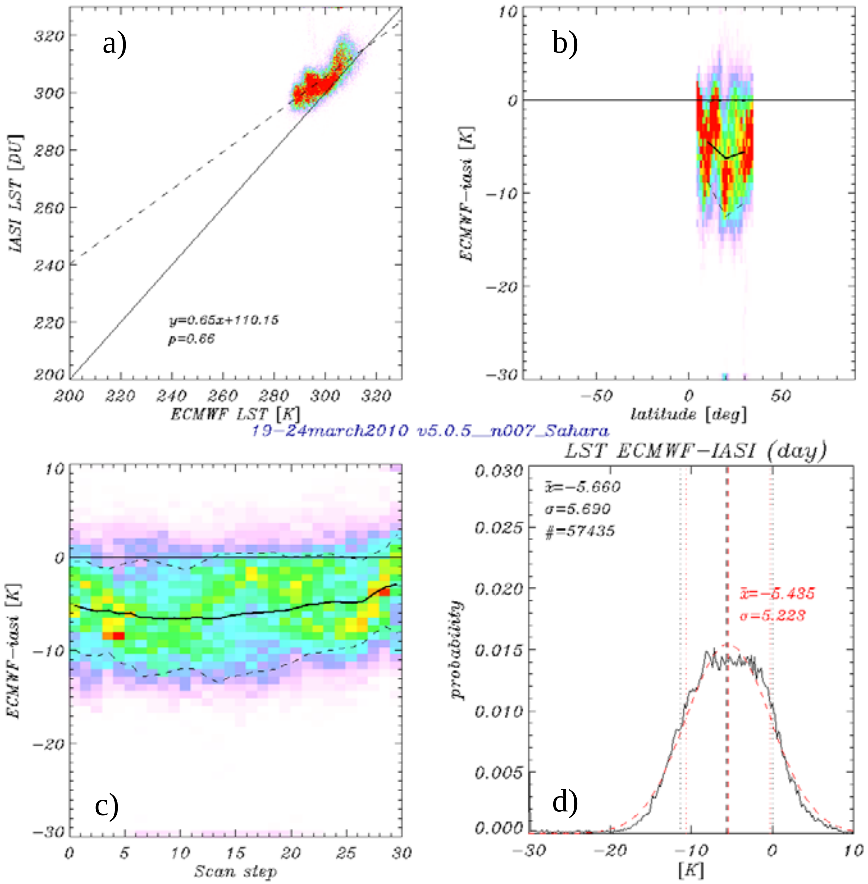

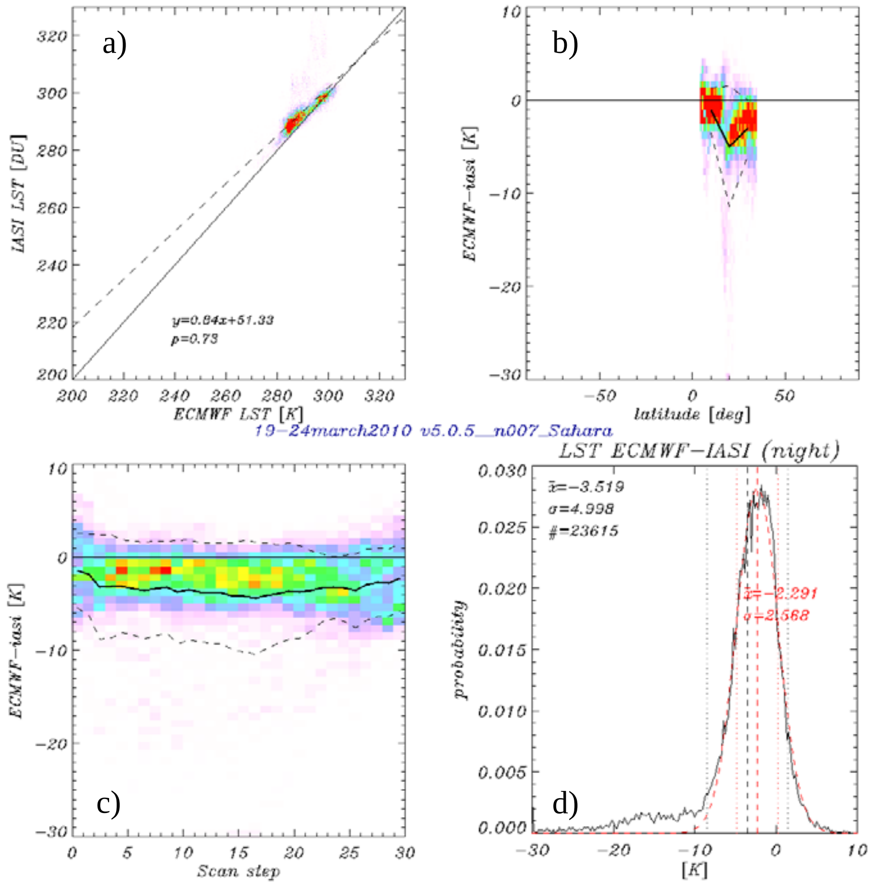

***Figure 30:** Same as **Figure 29**, for the Sahara only*

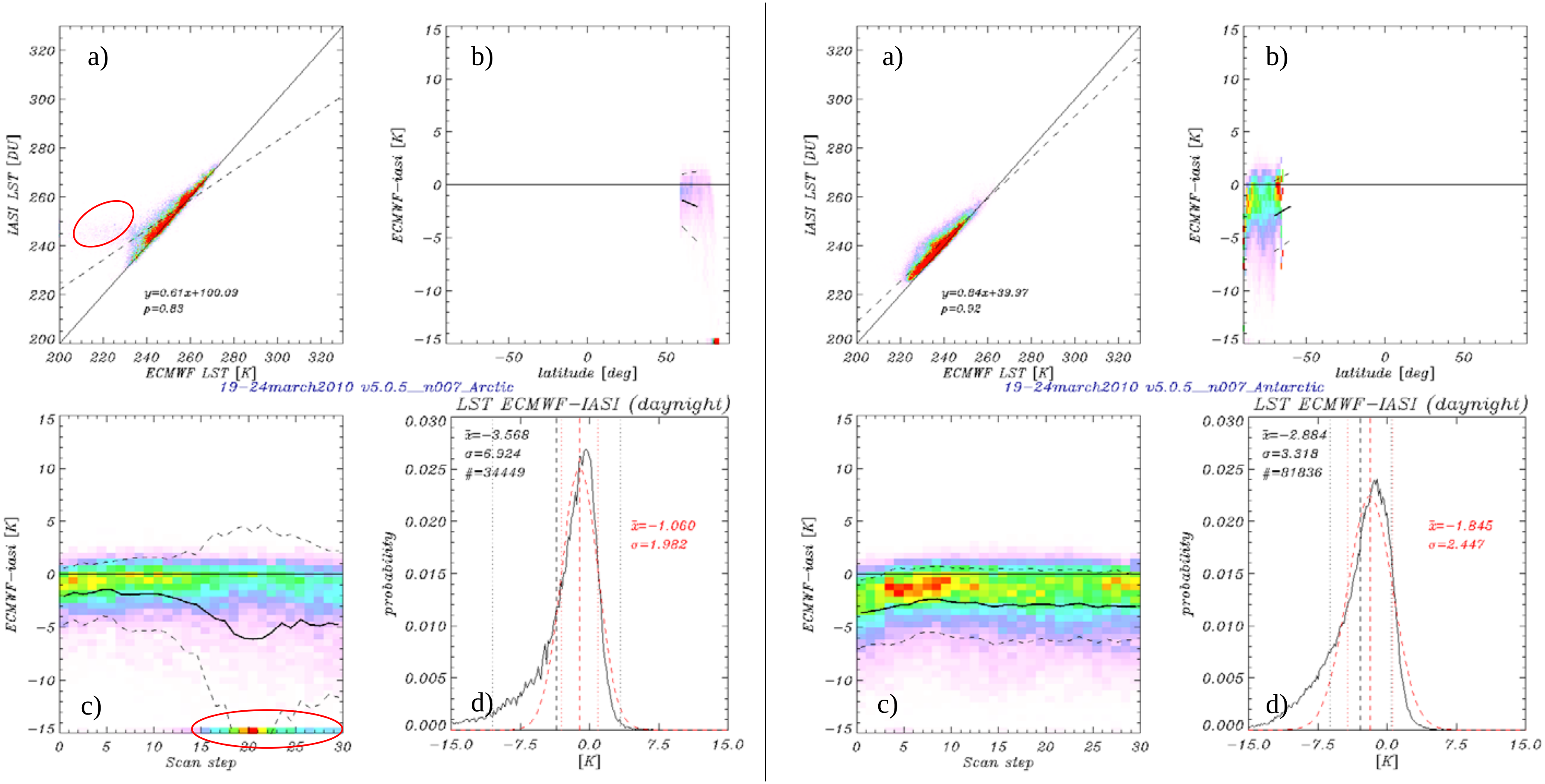

Figure 31: *Same as* ***Figure 29****, for the Arctic (left) and Antarctica (right)*

3.2.4 ECMWF – PPF v4.3, 19-24 March 2010

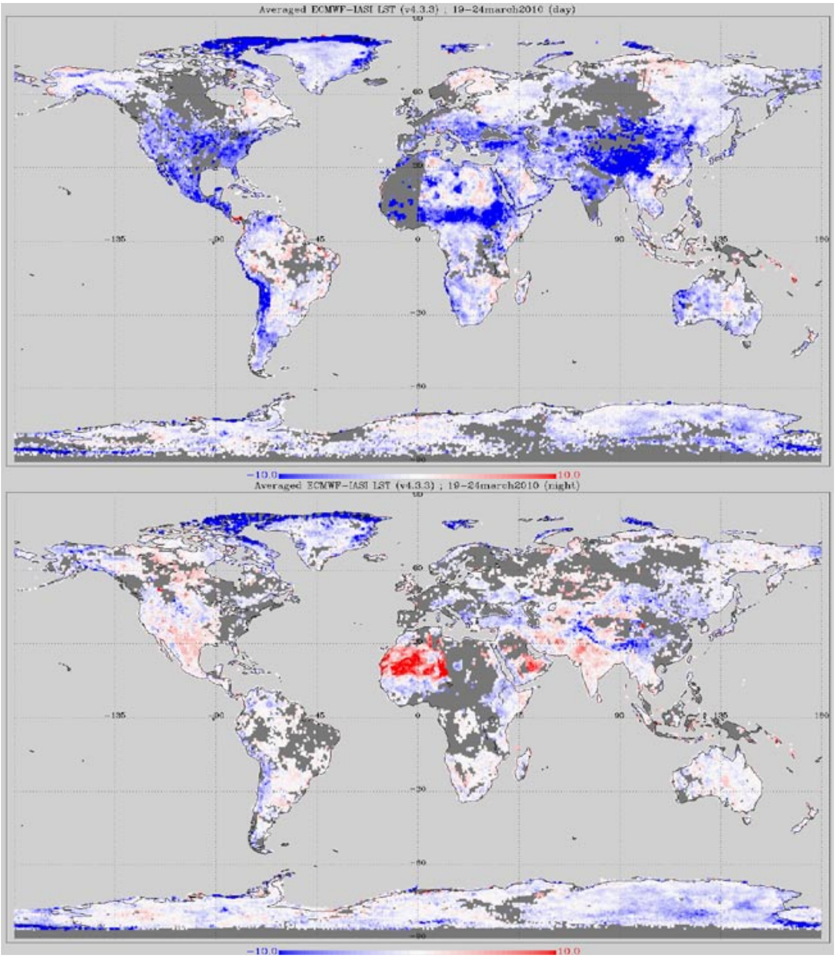

Figure 32: *Mean departures for day (top) and night (bottom)*

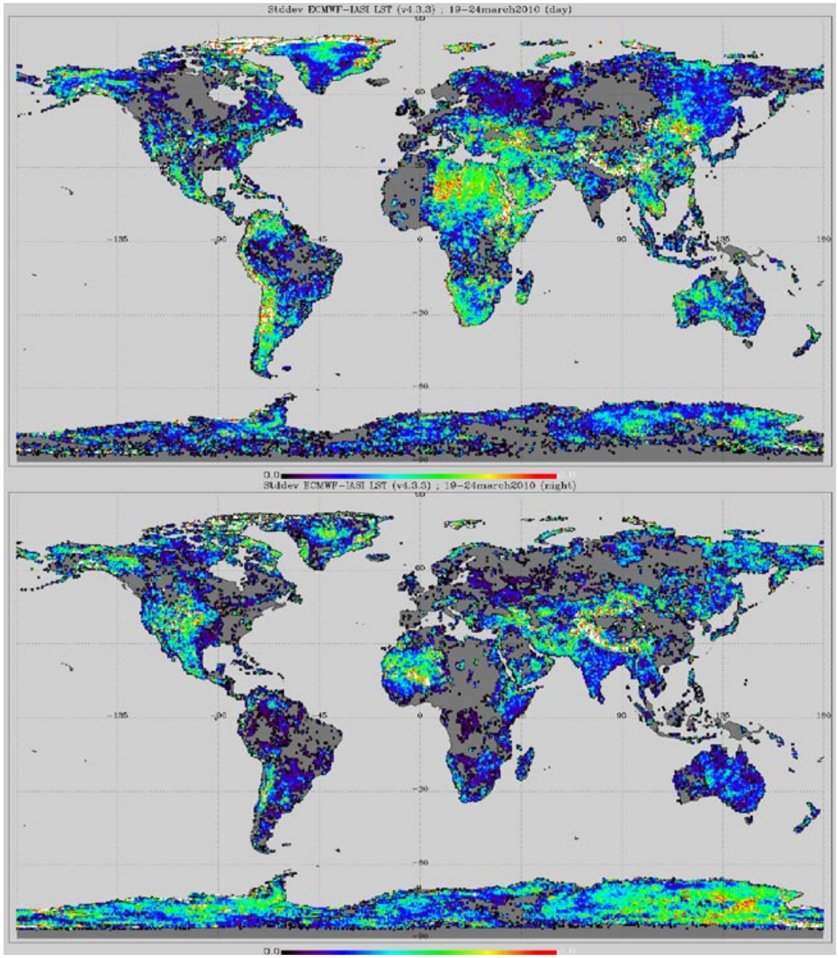

Figure 33: *Error standard deviations for day (top) and night (bottom)*

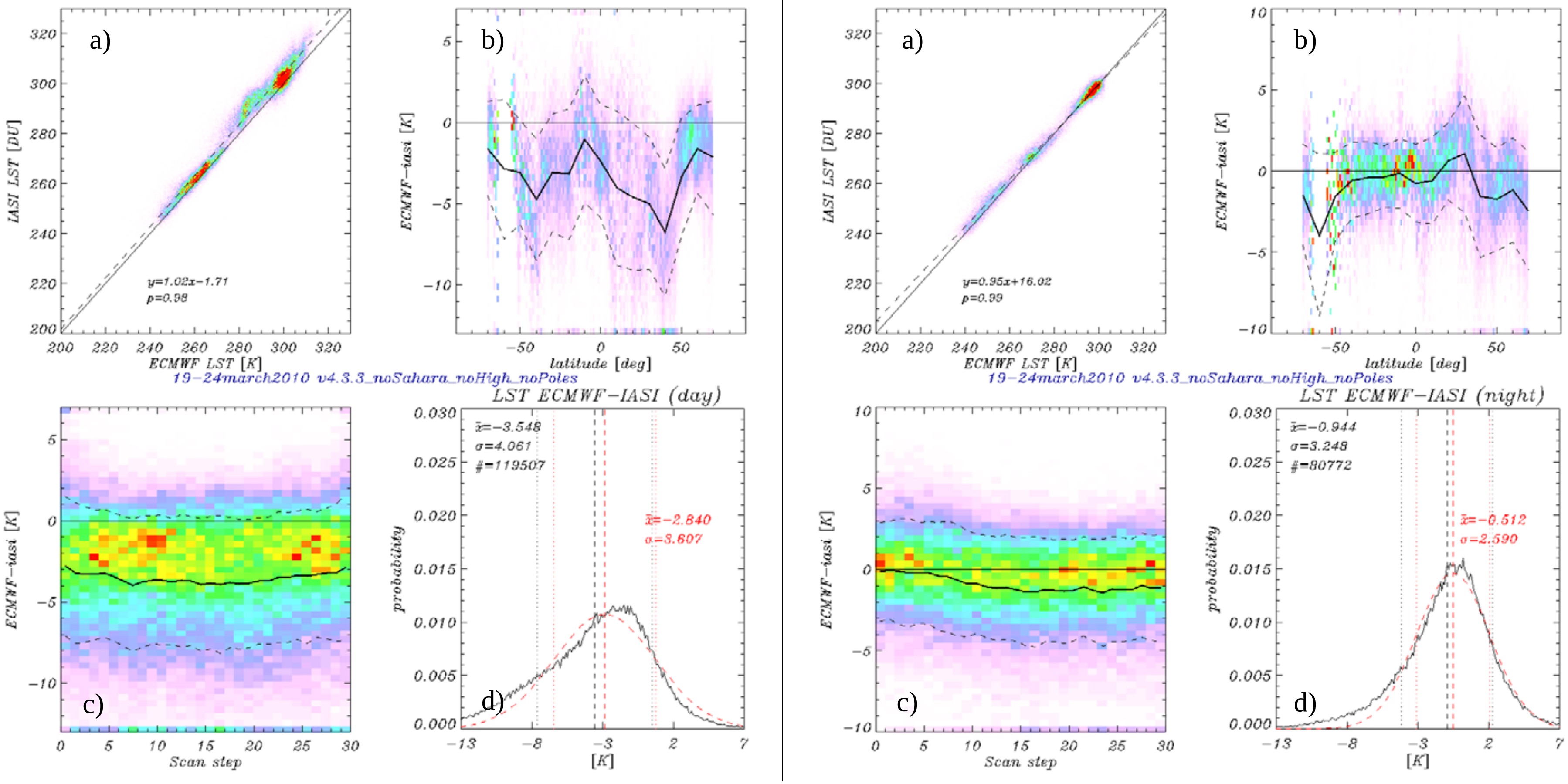

Figure 34: *Correlation (a) and statistics (d) of ECMWF – IASI (PPF v4.3) LST departures and their variations with latitude (b) and scan angle (c) for day- and night-times (left and right panels, respectively). Sahara, polar and elevated regions (Ps<800 hPa) were excluded.*

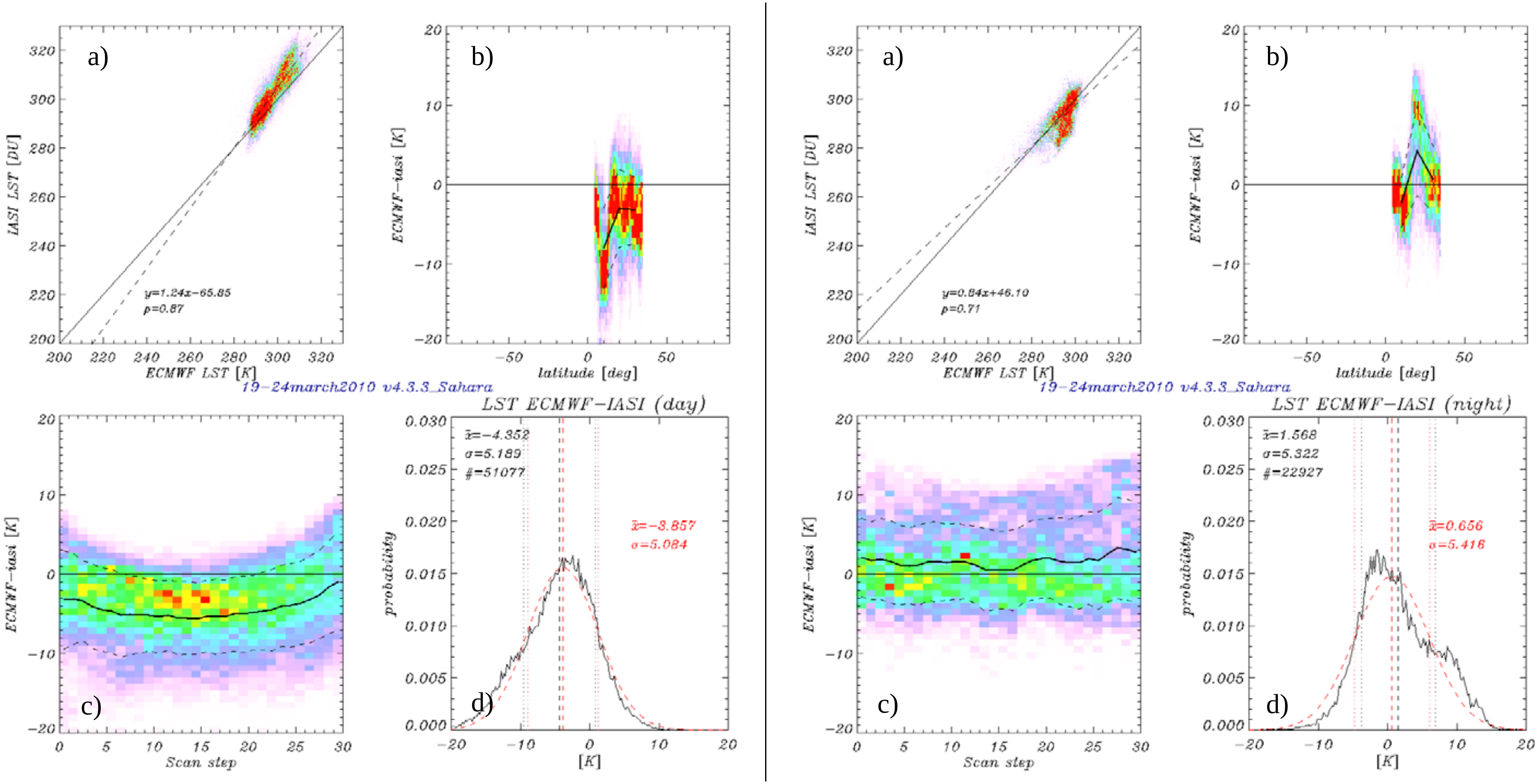

Figure 35: *Same as Figure 34, for the Sahara only*

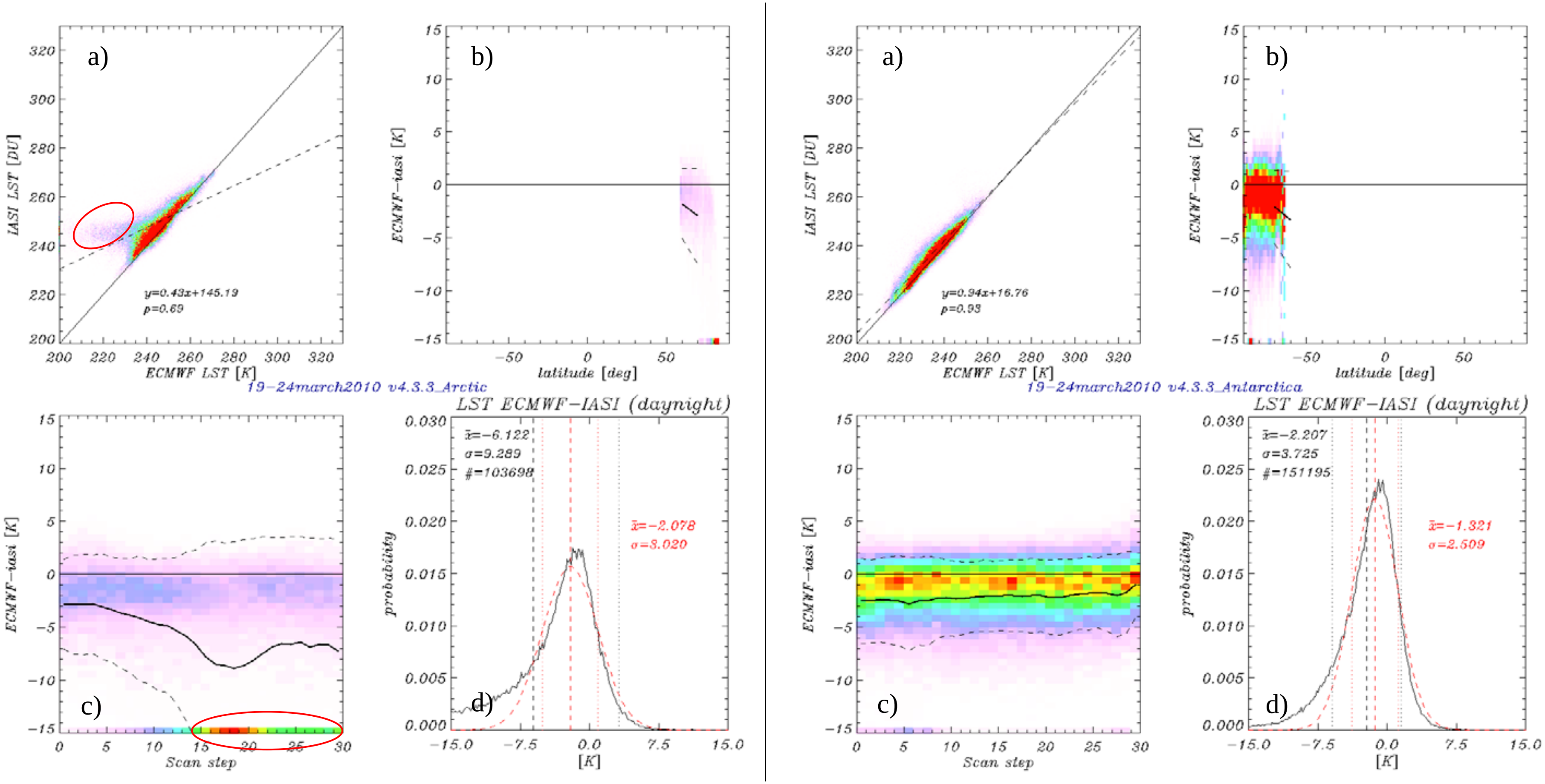

Figure 36: *Same as Figure 34, for the Arctic (left) and Antarctica (right)*

4 DISCUSSION ON IASI LST PERFORMANCES AND ERRORS

4.1 General Figures

The comparisons of the three IASI retrievals with the two references, LSA and ECMWF, present different characteristics which are summarised in Table 1. The best agreements are usually achieved with the LSA SAF products at night, where the respective departures are closer to Gaussian distributions and the rms errors amount to about 2 K. The correlation between the retrieved LST and the references for non-polar latitudes and non-arid surfaces is very high, from 0.97 to 0.99.

The largest discrepancies occur over arid regions such as the Sahara and over elevated as well as polar regions. They mostly affect the statistical methods (PPF v4 and PPF v5 FG) with typical departures of up to 15 K, with some specific higher errors in the Rub Al' Khali region (Arabian Peninsula) for instance. (Deserts are addressed in more detail in Section 4.4.) The characterisation of the infrared surface emissivity is a known critical issue with these bare soils and we therefore treated the tropical and temperate latitudes separately. Elevated regions with surface pressure lower than 800 hPa, like the Himalayas and the Andes, are sources of large deviations and have also been excluded from the global comparison with ECMWF. The different spatial resolutions of the LST products (IASI footprint and model grid) in comparison to the variability scale of the local topography do not allow a direct intercomparison. As for the polar caps and especially Antarctica, the model analyses agree best of all with the EOF regressions (PPF v4 and PPF v5 FG) in terms of bias. The error standard deviations over the South Pole are similar for all three retrieval algorithms tested here, of about 3.5 K, and are comparable to the global figures. These conclusions largely apply to the North Pole with the exception of the most northerly islands and Greenland coasts. Very strong outliers, still under investigation, are observed there where ECMWF is up to 30 K colder (see red circles in Figure 26, Figure 31 and Figure 36) and which similarly affect all three methods.

At night-time, the absence of solar illumination allows a direct comparison of the LST retrieved or modelled from different instruments, which otherwise is also a function of the Sun – surface – instrument relative geometry because of the shadows due to, for instance, the orography or the vegetation. For a given place and time, the higher the alignment between the instrument, the Sun and the scene, the smaller is the observed shadow fraction and the warmer is the sensed LST. During this 6-day period in March, over non-polar, elevated or arid regions, all three methods show a small warm bias from the LSA products, of 0.4 K with version 4, 0.8 K with the OEM (v5) and 1.6 K with the first guess in version 5. Addressing a similar population of about 10^3 cases, the respective standard deviations are similar and below 2 K, which for the PPF v4 is consistent with the initial validations performed against MODIS [RD 2]. During daytime, these biases remain similar for the PPF v4 and v5 FG while the v5 OEM becomes colder by 2 K on average. The standard deviations consistently slightly increase to about 2.5 K. As a general trend, the departure distributions present a thinner peak for the two statistical methods than the OEM in v5, but with a few stronger outliers.

			Day		Night	
			Bias	σ	Bias	σ
LSA-IASI	V5 OEM	No Sahara	2.0 (2.1) K	2.4 (2.1) K	-0.8 (-0.7) K	1.8 (1.7) K
		Sahara	2.3 (2.7) K	3.0 (2.8) K	-1.2 (-1.4) K	2.2 (2.1) K
	V5 FG	No Sahara	-0.6 (-0.7) K	2.4 (1.8) K	-1.6 (-1.2) K	1.6 (1.0) K
		Sahara	-1.7 (-1.3) K	4.6 (3.3) K	-4.4 (-2.9) K	5.6 (3.0) K
	V4	No Sahara	-0.3 (-0.2) K	2.7 (2.0) K	-0.4 (-0.2) K	1.6 (1.2) K
		Sahara	1.5 (2.5) K	6.4 (6.4) K	1.8 (1.0) K	5.2 (4.2) K
ECMWF-IASI	V5 OEM	No (high, Poles, Sahara)	-1.6 (-1.3) K	3.0 (2.6) K	-1.5 (-1.0) K	3.2 (2.7) K
		Sahara	-2.4 (-2.4) K	3.2 (3.4) K	-1.2 (-1.0) K	2.4 (2.1) K
		Poles (Antarctica, Arctic)	-4.8 (-3.7) K	3.1 (2.3) K	-5.6 (-3.1) K	7.2 (2.4) K
	V5 FG	No (high, Poles, Sahara)	-4.0 (-3.2) K	3.6 (3.1) K	-1.9 (-0.9) K	2.9 (1.7) K
		Sahara	-5.7 (-5.4) K	5.7 (5.2) K	-3.5 (-2.3) K	5.0 (2.6) K
		Poles (Antarctica, Arctic)	-2.9 (-1.8) K	3.3 (2.5) K	-3.6 (-1.1) K	6.9 (2.0) K
	V4	No (high, Poles, Sahara)	-3.5 (-2.8) K	4.1 (3.6) K	-0.9 (-0.5) K	3.2 (2.6) K
		Sahara	-4.4 (-3.9) K	5.2 (5.1) K	-1.6 (-0.7) K	5.3 (5.4) K
		Poles (Antarctica, Arctic)	-2.2 (-1.3) K	3.7 (2.5) K	-6.1 (-2.1) K	9.3 (3.0) K

Table 1: *Statistics summary of the respective (Reference–IASI) LST departures for the 19-24 March 2010 period. In parentheses: the biases and standard deviations of the main Gaussian mode.*

Although no absolute calibration can be inferred from it, it is interesting to note that the same conclusions qualitatively apply to the intercomparison with the ECMWF analyses. The standard deviations at night-time are indeed comparable for all three methods (~3 K) and the (warm) biases, though translated by half-a-degree, rank the same way: PPF v4 (0.9 K) then PPF v5 OEM (1.5 K) and PPF v5 DZ (1.9 K). In daytime, the biases become as high as 4 K and the standard deviations increase as well to 3.0, 3.6 and 4.1 K for PPF v5 OEM, PPF v5 DZ and PPF v4 respectively.

It must be noted here also that in some areas the OEM implemented in the PPF version 5 did not offer counterparts to the other two methods, as for instance in the Sahel where the iterative process rarely converged, with the result that no LST was available despite the identification of clear pixels. The Sahel is the semi-arid transition zone between the Sahara to the north and the first tropical forests to the south. Mostly covered in grassland and savanna, with areas of scattered trees and shrubland, a complex surface emissivity could be invoked to explain the behaviour of the OEM although no specific studies have been carried out so far. On the contrary, retrievals are essentially always available from the EOF regressions if they are attempted. In this area particularly, the LST retrieved with the PPF v4 significantly deviated from the LSA SAF and ECMWF products.

4.2 Scan Angle Dependency

The variation of the LST errors with the scan angle was specifically studied and is represented in the lower left corner of each quadruple in Figure 12 to Figure 36. It can be best assessed in the absence of sunlight to avoid the superposition of the geometrical effects due to the surface illumination. During daytime indeed, IASI, scanning westwards in the morning, will sense surfaces with decreasing shadow fractions. Assuming to the first order a constant shadow fraction for SEVIRI within the IASI swath, the difference from the LSA LST is then expected to decrease, which is confirmed by the daytime plots for non-Saharan situations in Figure 12, Figure 16 and Figure 20 where the departures drop by 2 to 3 K from one swath edge to the other. Comparisons with ECMWF carry higher intrinsic errors in the reference data which are believed to mask out this geometrical effect.

At night-time however, any angular variations can be directly associated with the retrieval scheme itself. For non-desert soils, a small variation not exceeding 1 K is present in PPF v4 LST products from the nadir to the limit of the swath, while the profile of the departures remains perfectly flat with the v5 FG (Figure 16 – night). The (LSA SAF – PPF v5 OEM) departures however exhibit a noticeable variation of about 2.5 K from the middle to the end of the measurement line (Figure 12 – night). With the PPF v5 OEM, the amplitude of this variation is much higher when it comes to the Sahara, of approximately 5 K regardless of the local time. With the two statistical retrievals it is consistently as high at daytime but disappears for night cases.

4.3 Variation with the Surface Elevation

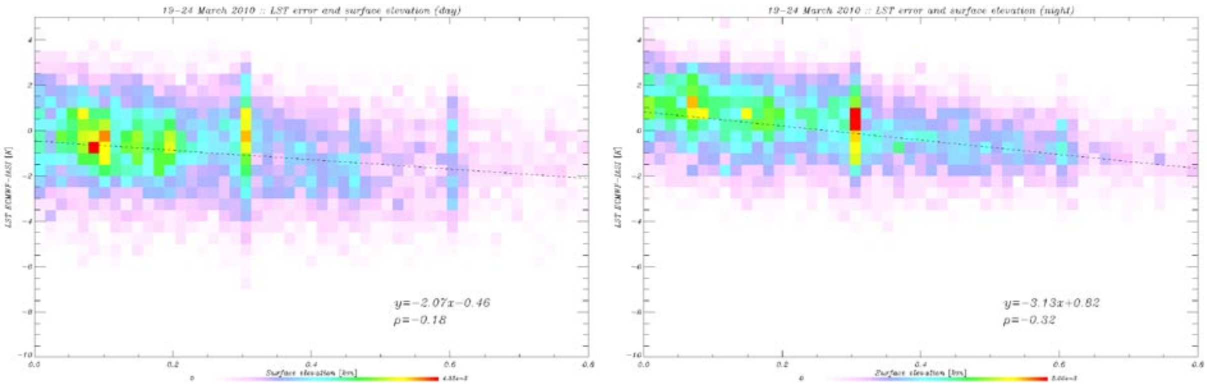

Figure 37: *Variation of the (ECMWF – IASI v5 OEM) LST difference with the surface elevation for day (left) and night (right) in the first 800 m*

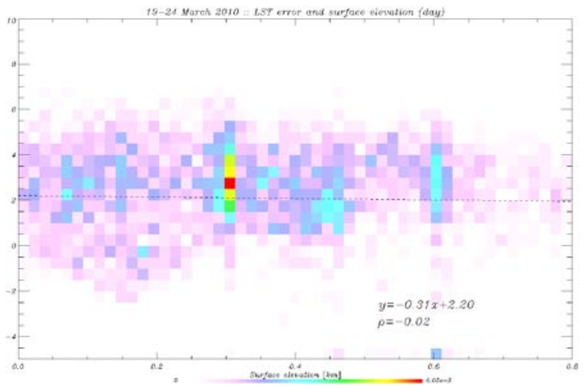

Figure 38: *(LSA SAF – IASI v5 OEM) LST difference vs. surface elevation at daytime in the first 800 m*

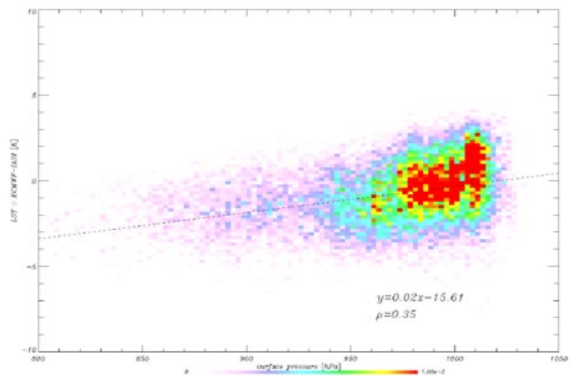

Figure 39: *Variation of the (ECMWF – IASI v5 OEM) LST difference with the surface pressure*

As illustrated by Figure 37 and Figure 39, the mean LST errors in the PPF v5 OEM, assessed with the ECMWF analyses, have a slight correlation with the surface elevation, decreasing at a rate of about 2 to 3 K/km or 2 K/100 hPa. These observations were made with day and night retrievals during the period 19-24 March 2010 for altitudes below 1000 m, with the exclusion of latitudes above 70°. For higher surfaces, this trend was no longer observed. A similar study was repeated with the LSA SAF products where LST errors and surface elevation appear to be completely decorrelated (Figure 38) which suggests that the variation with the surface elevation is essentially coming from the modelled LSTs.

4.4 The Rub' Al Khali Desert

In general, the departures with PPF v4 over the Sahara present large variability, ranging between -15 and 15 K, especially at night-time. The spread is however much smaller with the FG and OEM of revision v5, but a few sub-regions are subject to unrealistic outliers with the v5 FG, where associated LSTs can be 20 to 30 K warmer than the references, especially at night (green ellipses in Figure 40 and Figure 41). A brief case study was conducted on the Arabian Peninsula and more precisely on the sub-region named Rub' Al Khali which very well illustrates these observations. This is an extreme arid area south of Saudi Arabia (Figure 42) with fine sand dune structures running over rocky and salty darker flats (see Figure 43).

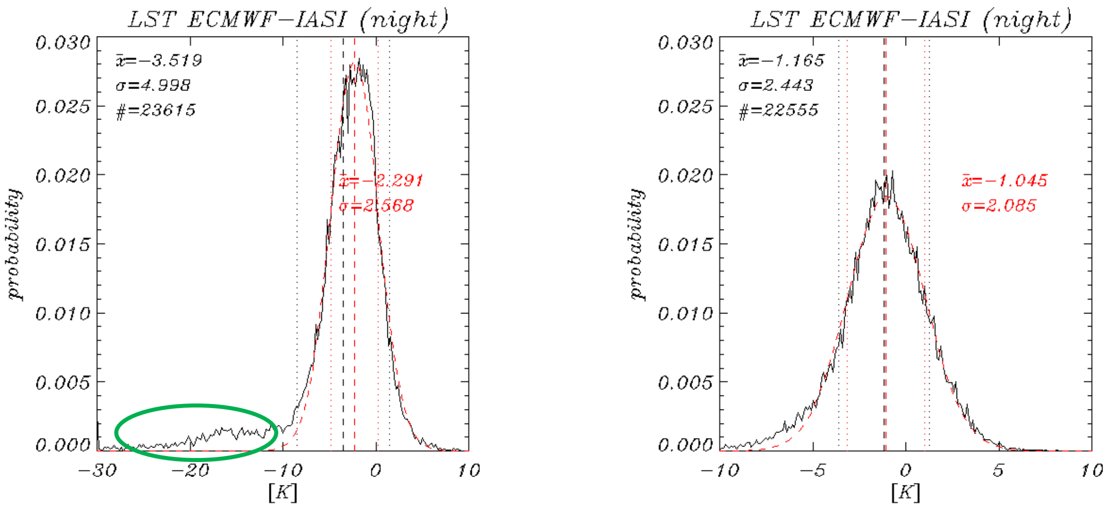

***Figure 40:** ECMWF–IASI LST distributions at night over the Sahara and Arabia during the 19-24 March 2010 period for PPF v5 FG (left) and OEM (right)*

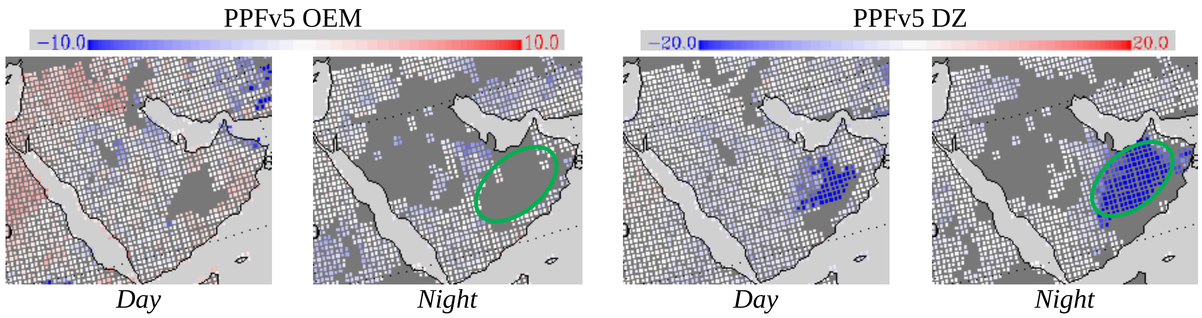

***Figure 41:** Mean (LSA–IASI) LST*

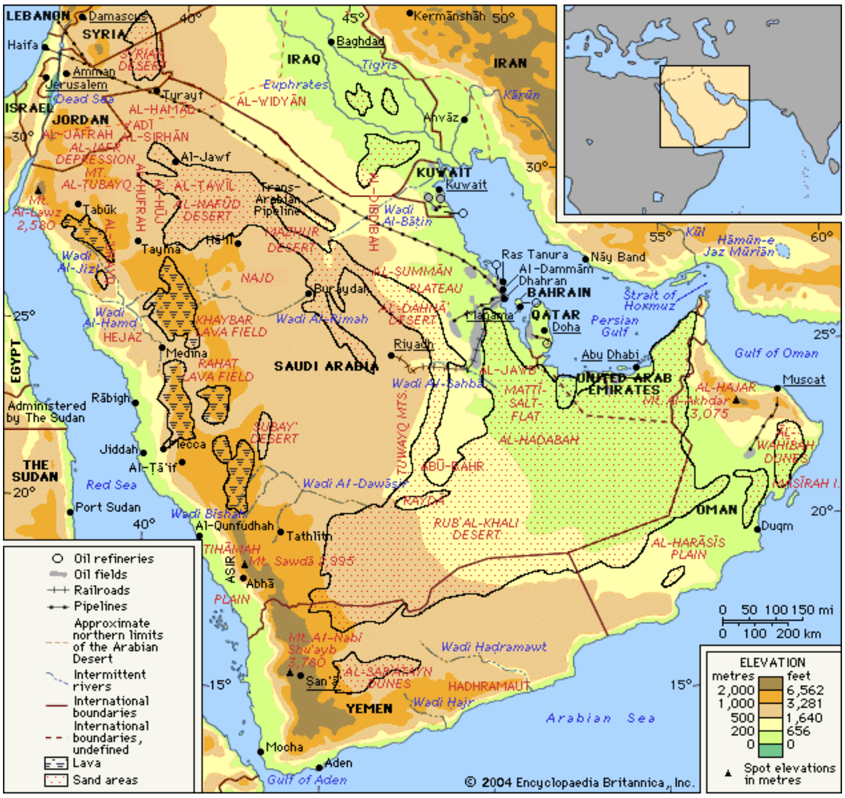

Figure 42: *Geophysical map of Saudi Arabia (Encyclopaedia Britannica)*

Figure 43: *Close-up view of the Rub' Al Khali with ASTER/Terra (NASA)*

At first sight, the products generated with the v5 OEM do not exhibit these large departures (Figure 40, right), which is actually due to the absence of retrievals in this area rather than to more accurate products. A closer inspection of the flags FLG_IASICLD and FLG_RESID, which respectively indicate the cloudiness and the success of the iterative retrieval, indicates that the Rub' Al Khali is usually not covered by clouds (white pixels in Figure 45, left) but that the state vector resulting from the OEM is eventually discarded (white pixels in Figure 45, right).

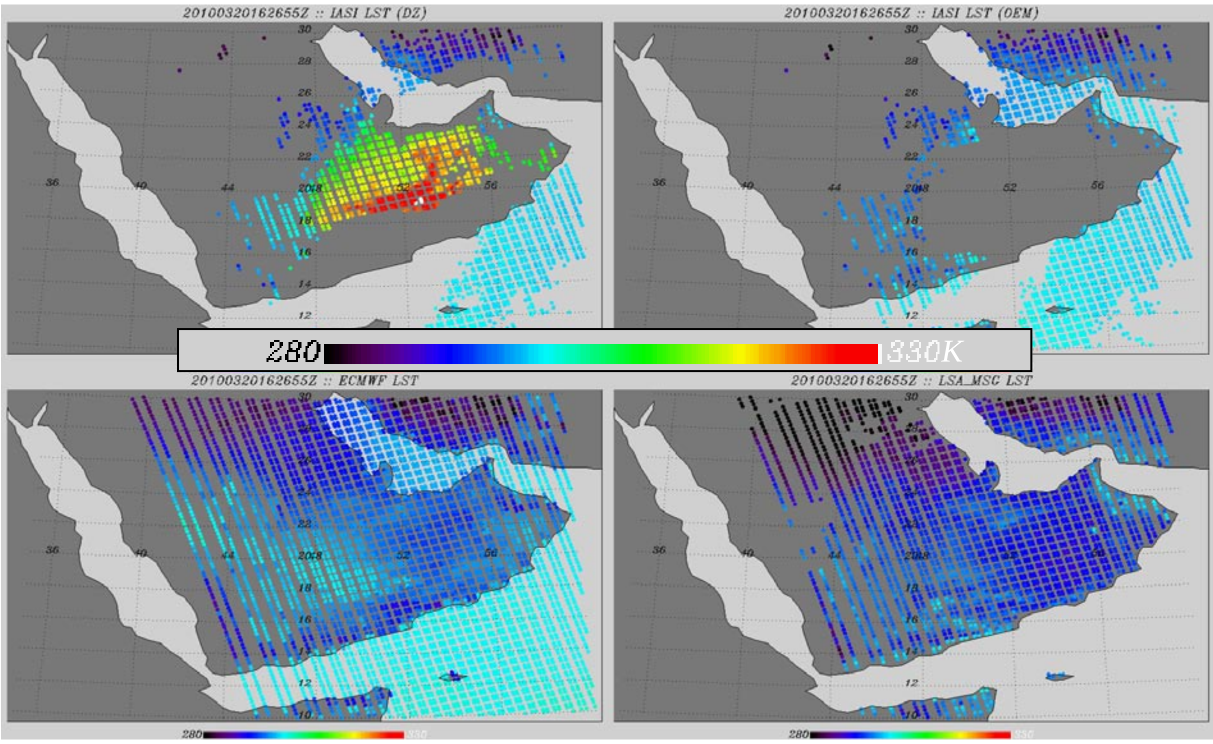

Figure 44: *LST on 20 March 2010 in the evening as retrieved with IASI v5 FG (upper left), v5 OEM (upper right), ECMWF (lower left) and LSA MSG (lower right)*

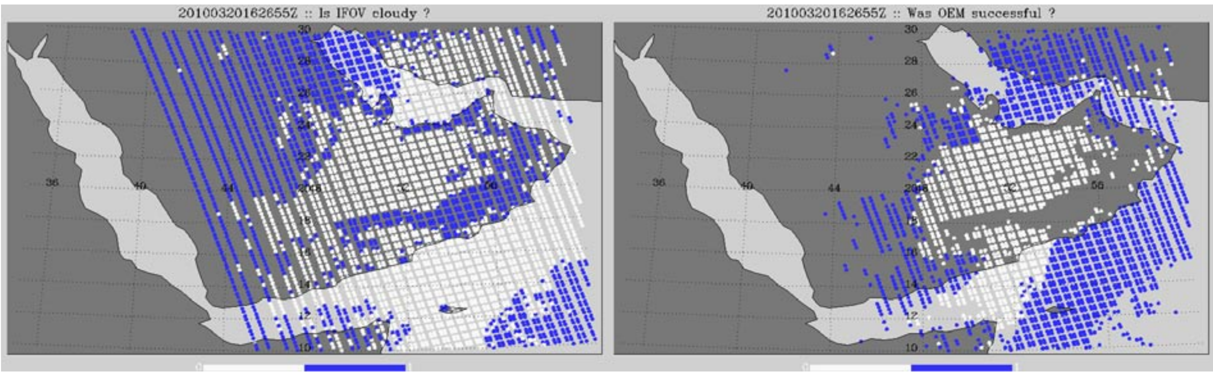

Figure 45: *Cloudiness (left) and successful convergence of the OEM assessed in the v5 OEM run. White stands for "no" and blue for "yes".*

The absence of LST in this area with the PPF v5 OEM applies to every day in the studied period 19-24 March 2010, while the large departures resulting from the v5 FG did not systematically occur. On the 19th for instance, the retrieved LST were closer to the ECMWF and LSA products than on the following days when high divergences took place (Figure 48). A visual inspection in the AVHRR channel 4 images shows that different structures are visible from one day to the next in that area (dashed lines in Figure 46), which could betray the presence of aerosols like dust or sand in the atmosphere and would account for the corrupted LSTs retrieved with the first guess. A monitoring of the area over a longer period would be necessary to identify the root cause of the large errors with the FG and the rejections occurring with the OEM. A possible explanation could reside in very peculiar surface properties in the IR whose emissivities are not necessarily well represented and characterised in the training and retrieval databases. It is also interesting to note in that respect that the LSA products and the time-interpolated ECMWF analyses show large differences, ranging between -5 and more than 10 K for the Arabian Peninsula alone (Figure 49).

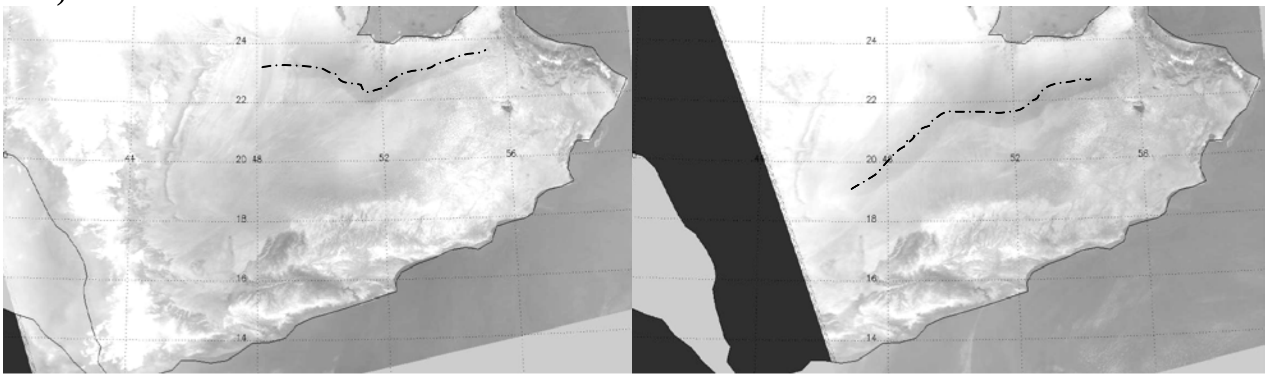

Figure 46: *Changing structures in AVHRR channel 4 images (reverse video) of the Rub' Al Khali on 20 (left) and 21 (right) March 2010, evening overpasses*

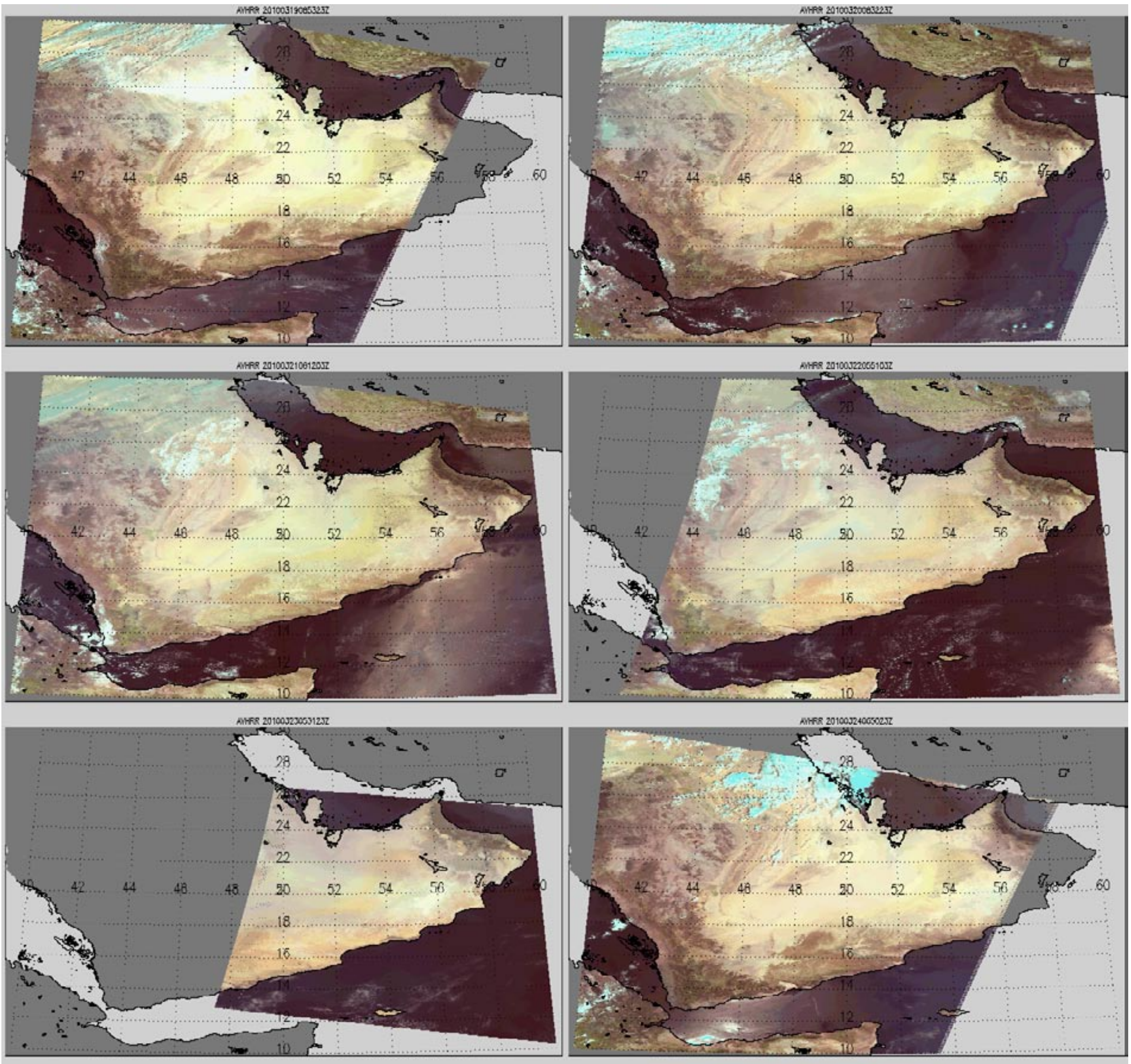

Figure 47: *Time series of AVHRR RGB (VIR1.6 µm, VIS0.8 µm, VIS0.6 µm) composite, 19-23 March 2010 on evening overpasses, from left to right and top to bottom*

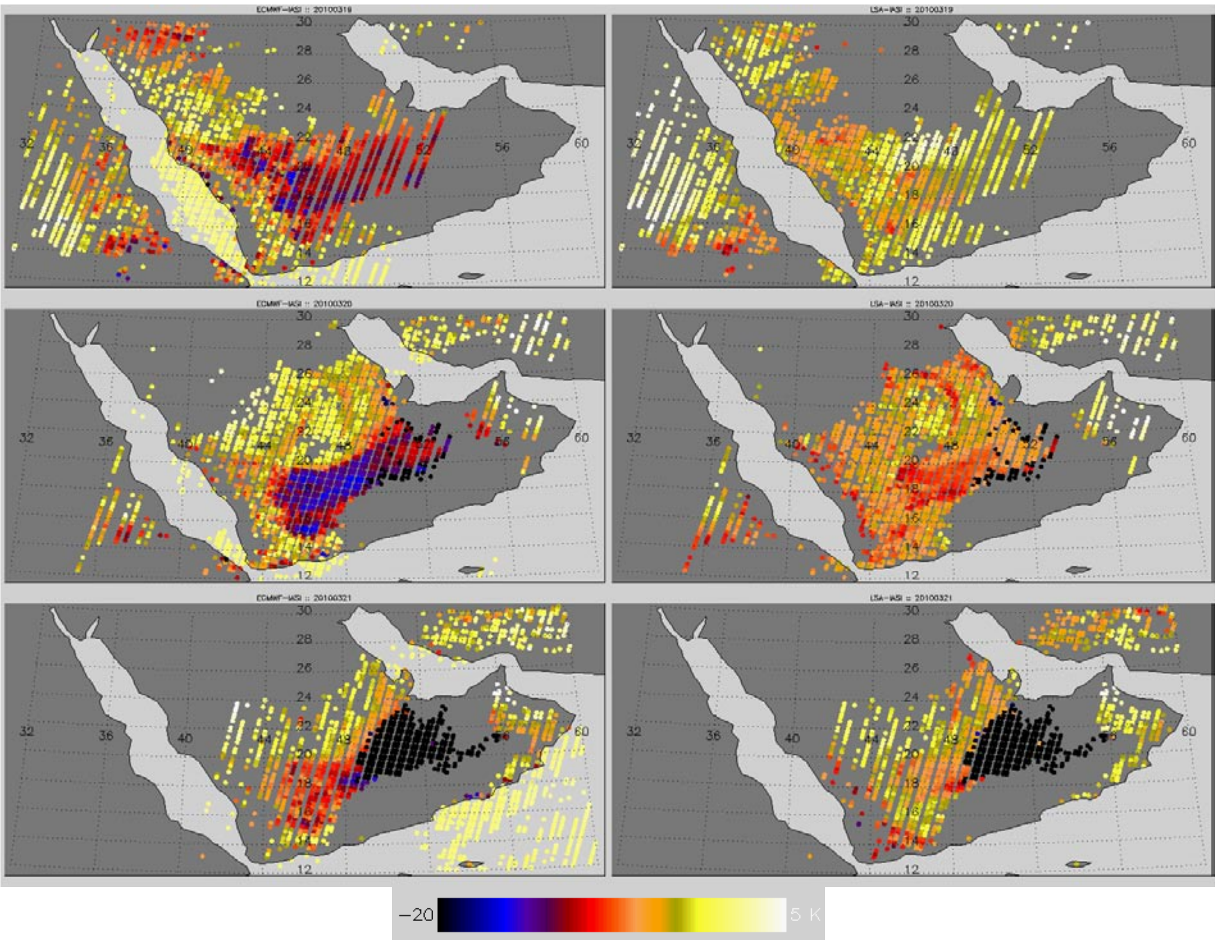

Figure 48: *Time series of IASI LST departures from ECMWF (left) and LSA SAF (right) products at daytime on 19, 20 and 21 March 2010 from top to bottom, respectively*

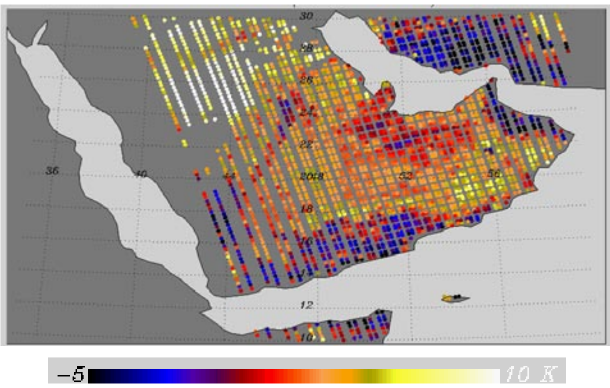

Figure 49: *(ECMWF – LSA) LST collocated to IASI IFOVs on 20 March 2010, evening pass*

5 SUMMARY AND CONCLUSIONS

The SST and LST products of the latest IASI L2 PPF version, namely version 5, have been compared against external satellite products generated from the instruments AATSR and SEVIRI, respectively. These reference products had been validated against in-situ measurements, with typical errors of about 0.3 K (AATSR SST) and 2 K (SEVIRI LST) such that the intercomparisons presented in this document may support the validation of the IASI surface temperatures. ECMWF analyses were also used as reference products to extend the validation to places which were not covered by the AATSR/IASI and SEVIRI/IASI collocations. They are however assumed to be of lower quality than the satellite products, with typical errors of 1 and 5 K associated with SST and LST respectively. Ultimately, the IASI L2 SST quality has been monitored against AVHRR and buoys data.

Regarding the SST, the only change in the retrieval algorithm since version 4 is the processing of noise-filtered radiances. A cold bias of 0.3 to 0.4 K was characterised and the error standard deviation is usually lower than 0.5 K, which confirms an initial validation study performed in 2008. The retrieval is, however, sensitive to the tropospheric water-vapour content and higher errors were characterised by humid atmospheres. Additionally, the current cloud detection algorithms in the IASI L2 PPF v5 do not identify the presence of aerosols and we could qualitatively correlate dust loads with larger SST errors, of up to a few kelvin, off the Western African coasts and over the Arabian Sea for instance. Eventually, a small angular dependence on the SST error was characterised, with an increase of approximately 0.3 at the largest viewing angles.

As for the LST, the retrievals result from an optimal estimation method in the IASI processing chain version 5 while this parameter was retrieved from a regression with the spectral principal components in v4. Both methods, as well as the statistical first guess of v5, another EOF regression, were tested against land surface temperatures produced at the LSA SAF with SEVIRI measurements and against ECMWF analyses. The best match is obtained at night with LSA SAF products for areas which exclude elevated surfaces, the Sahara and the North Pole. All three products present similar error standard deviations, of about 1.7 K, with slightly different biases of 0.4, 0.8 and 1.6 K for v4, v5 FG and v5 OEM, respectively. The results obtained with v4 are consistent with a previous validation study performed with MODIS LST products [RD 2]. The overall quality is slightly worse in Antarctica, with error standard deviations of 3.1 to 3.7 K for all three methods when compared to ECMWF, and with larger biases. Over bare arid soils such as the Sahara, the v5 OEM presents the best statistics but systematically rejected the retrievals in specific sub-regions like Rub' Al Khali during the studied period, where the v5 FG and the reference products diverged noticeably. A variation of 2.5 K in the mean LST errors characterises the v5 OEM retrievals for non-desert surfaces, which is consistent with some angular dependency reported in the retrieved temperature on the boundary levels [RD 19]. This feature reaches up to 5 K in the Sahara. The v5 FG retrievals are however not affected by such scan angle dependency. Considering that they otherwise present similar statistics as the v5 OEM, one could therefore advantageously substitute the v5 FG into the operational L2 products for all IFOVs where the OEM converged.

In general, for both the SST and the LST, some further validation work has to be done to confirm the results over a longer period. The detection of aerosols would allow flagging the quality of the surface temperatures, and further specific investigation and validations are needed to achieve consistent LST retrieval in some singular arid sub-regions and on elevated surfaces.